TRIBHUVAN UNIVERSITY

INSTITUTE OF ENGINEERING

PULCHOWK CAMPUS

THESIS NO.: M-350-MSREE-2018-2022

Impact of Photovoltaic Generation in the System Stability:

A Case Study with Nuwakot PV

by

Pravin Chaudhary

A THESIS

SUBMITTED TO THE DEPARTMENT OF MECHANICAL AND AEROSPACE ENGINEERING IN PARTIAL FULFILLMENT OF THE REQUIREMENTS FOR THE DEGREE OF MASTER OF SCIENCE IN RENEWABLE ENERGY ENGINEERING

DEPARTMENT OF MECHANICAL AND AEROSPACE ENGINEERING

PULCHOWK CAMPUS

LALITPUR, NEPAL

SEPTEMBER, 2022

Impact of Photovoltaic generation in the system stability: A case study with Nuwakot PV

By

Pravin Chaudhary

(PUL074MSREEE010)

Thesis Supervisor

Shahabuddin Khan

Asst. Professor

Department of Electrical Engineering

Pulchowk Campus

A Thesis submitted to the Department of Mechanical and Aerospace Engineering in partial fulfillment of the requirements for the Degree of
Master of Science in Renewable Energy Engineering

Department of Mechanical and Aerospace Engineering

Institute of Engineering, Pulchowk Campus

Tribhuvan University

Lalitpur, Nepal

September, 2022

COPYRIGHT

TRIBHUVAN UNIVERSITY

INSTITUTE OF ENGINEERING

PULCHOWK CAMPUS

DEPARTMENT OF MECHANICAL AND AEROSPACE ENGINEERING

Certificate of Approval

The undersigned certify that they have read, and recommended to the Institute of Engineering for acceptance, a thesis entitled " **Impact of Photovoltaic generation in the system stability: A case study with Nuwakot PV**" submitted by **Pravin Chaudhary** in partial fulfillment of the requirements for the degree of Master of Science in Renewable Energy Engineering.

_____

Supervisor, Shahabuddin Khan
Asst. Professor
Department of Electrical Engineering
IOE, Tribhuvan University

_____

External Examiner, Dr. Samundra Gurung
Asst. Professor
Department of Electrical and Electronics Engineering
Kathmandu University

_____

Committee Chairperson, Dr. Surya Prasad Adhikari
Head of Department
Department of Mechanical and Aerospace Engineering
IOE, Tribhuvan University

Date: 18 September, 2022

ACKNOWLEDGEMENT

First of all, I would like to express my gratitude be thankful to my Supervisor, Asst. Prof. Shahabuddin Khan, Department of Electrical Engineering, Pulchowk Campus, Tribhuvan University. I was really fortunate that I had the kind association as well as his supervision. His exemplary guidance, constant encouragement, and careful mentoring throughout the thesis work are so great that even my profound gratitude is not enough. I would like to express my due respect to, Dr. Hari Darlami and Dr. Surya Prasad Adhikari for their care, encouragement and valuable suggestion for the thesis work.

I would like to extend my gratefulness to Transmission and Generation directorate, NEA for providing support with the data and elaboration required for the modeling of the system and their guidance in the process of the thesis work.

Moreover, I acknowledge with thanks for the timely guidance and loving inspiration, which I have received from my family without whom this task would have been challenging for me.

I would like to take this opportunity to express a deep sense of gratitude to all friends family members, and teachers of the Department of Mechanical and Aerospace engineering and Electrical engineering who have provided their valuable support, suggestions and guidance in the research work.

ABSTRACT

As innovation drives costs lower and begins to fulfill the promise of a clean energy future, renewable energy is rising. Renewable energy sources like PV and wind are taking on greater significance as a source of power as we discover more inventive and affordable ways to capture and store wind and alternative energies. Due to sunlight's accessibility, solar PV systems may be used practically anywhere in the world. Traditionally it was assumed that, the grid inertia is sufficiently high with some small variations with respect to time. But this is not valid for the power system with high Renewable Energy Sources (RES) shares composed of PV and wind generations. The increase in the generation of the inertia-less system can cause different synchronization and stability issues along with the implication over frequency dynamics. So, the size of PV system to be injected to the system should be studied.

In this study, the simulation has been performed for the interconnected system encapsulating the Kathmandu valley, considering the scenario of injection of PV generation at Nuwakot. The load flow analysis before and after the placement of PV infers that the generation being placed away from the load center increases the overall network loss with minor change in the voltage at the nearby substations. The loss of the existing loss with 3.47%, with the placement of the PV at Nuwakot has increased to 3.97%.

The transient analysis indicates that when the PV suddenly isolates from the INPS, the voltage of the terminal bus of Devighat substation drops down to 0.954pu from existing 1.008pu. For the higher value of generation considered, the impact on the frequency and voltage is severe however is within the limits for the case of Nuwakot PV. In case of the synchronous system, with the increase in the generation voltage, for certain generation limits, the stabilization time reduces and the transient response would be gradual.

Finally, the small signal stability analysis with 0.1pu torque added in the generator at the Devighat confirms that the existing system is stable even due to the small disturbances. When the PV system was increased to 46MW capacity, the eigen value for the Mode 00046 and Mode 00047 was on the positive real axis with negative damping ratio indicating the system is unstable with some disturbances. However, the

system with synchronous generator is stable at 46MW generation. This indicates that the size of inertia-less PV generation needs to be studied for the integration with the INPS and the stability with the synchronous machine is higher as compared to the PV generations.

TABLE OF CONTENTS

LIST OF TABLES

LIST OF FIGURES

LIST OF ACRONYMS, SYMBOLS AND ABBREVIATIONS

CRSPP	Central Receiver Solar Power Plant
DC	double-circuit
DSL	DIgSILENT Simulation Language
GCPV	Grid-Connected Photovoltaic
GWh	gigawatt-hour
HP	Hydropower Plant
INPS	Integrated Nepal Power System
IS	International Standard
kW	Kilowatt
kWh	kilowatt-hour
LFA	Load Flow Analysis
MITS	Main Interconnected Transmission System
MW	Mega Watt
MWh	megawatt-hour
NEA	Nepal Electricity Authority
PR	Performance Ratio
pu	per unit
PV	Photovoltaic
RES	Renewable Energy Sources
SC	single-circuit
SG	Synchronous Generator
SLD	Single Line Diagram
SS	Substation

CHAPTER ONE: INTRODUCTION

1.1 Background

Renewable energy, often known as clean energy, is produced using replenishable natural resources or technologies (Shinn, 2018). As innovation drives costs lower and begins to fulfill the promise of a clean energy future, renewable energy is rising. Renewable energy sources are taking on greater significance as a source of power as we discover more inventive and affordable ways to capture and store wind and alternative energies. The use of renewable energy is growing on both large and small sizes, from enormous offshore wind farms to rooftop solar panels on houses that might sell power back to the grid. For lighting and heating, some rural communities even entirely rely on renewable energy.

The key strengths in the field of renewable energy to satisfy the anticipated plant capacity in the future are the harvesting actions of wind energy and solar energy. Due to sunlight's accessibility, solar PV systems may be used practically anywhere in the world, which gives them a significant advantage over wind energy systems, whose power generation is highly variable.(Khadka et al., 2020).

Nepal is blessed with sun radiation that ranges from 3.6 to 6.2 kWh/m²/day, with an average of 4.7 kWh/m²/day. In comparison to several European nations where PV systems have been extensively used, this intensity of irradiation is higher. The Upper Mustang region of Nepal receives the most solar radiation (6.16 kWh/m²/day)(*Global Solar Atlas*, 2022), which can be used by Grid-Connected Photovoltaic (GCPV) systems to produce power. Nepal also provides an added benefit for such a system. First off, as both the temperature and solar radiation rise with height (Panjwani & Narejo, 2014). Nepal has a larger potential for solar output because it is a mountainous and hilly country. Second, the price of PV technology has decreased by 80% or more since 2008 (IFC, 2015), which has led to a rise in interest in solar power recently.

The primary renewable source of electricity generation in Nepal is and has always been hydropower. The majority of hydropower is run-of-river and is dependent on glacier and monsoon melt, which lowers power output during the dry seasons (Gulagi et al., 2021). Even though with large hydropower potential, the power needs to be imported from India during the dry season and peak demand conditions. For a long time,

hydropower has been emphasized as the primary source of electricity to ensure continuous power and economic growth (Ogino et al., 2019). Due to their overreliance on one energy source, large hydropower projects, however, not only confront several social and environmental challenges but also technical and financial issues(Bogdanov et al., 2021).

The current utilization of the solar energy is negligible as compared to the available resource. The utilization of PV energy has been limited to some household lighting during outage of grid electricity, and use for some commercial buildings and study purpose and serve negligible amount in the generation in overall generation of the country. Though some commercial utilities have installed PV with inverter and net metering system with grid system of NEA, most of the consumers are still unaware of the effective utilization of PV. Till date, along with some mini-solar projects along with the Solar PV plant at Devighat has been installed by NEA.

The development of a large sized hydropower is challenging from both the financial and environmental aspects. Also, the development of the generating stations at various locations would be more desirable from the perspective of reduced loss and overall stability of the system. With the higher yielding capacity of Nepal, solar power generation can be considered to be an alternative. In the current scenario, where NEA is importing electricity at a much higher rate, the PV system with grid integrated can be more advantageous.

This thesis studies the impact of the grid connection of the inertia-less system considering the solar PV installed at Devighat, Nuwakot in the Integrated Nepal Power System (INPS) is performed. The impact on the voltage and loss with and without the system, together with the affect in the fault conditions and transient response on system inertia will be studied with the contingency analysis.

1.2 Problem Statement

Distributed generation has been considered as the measure for the improvement in system voltage and loss as well as system harmonics reduction. Also, the stability of the system is believed to be improved with the addition of DG. It was traditionally assumed that, the grid inertia is sufficiently high with some small variations with respect to time. But this is not valid for the power system with high Renewable Energy

Sources (RES) as PV and wind shares. With the integration of the 25MW PV generation at Nuwakot and various other PV generation at different location, the inertia-less energy is injected in the grid. This can cause different synchronization and stability issues along with the implication over frequency dynamics. So, the size of PV system to be injected to the system should be studied.

1.3 Research Objectives

Main objectives:

- To study the impact of Photovoltaic generation within interconnected system of Kathmandu valley

Specific objective:

- To analyze the voltage and loss of the INPS with and without the PV at Nuwakot
- To perform the transient analysis for the contingencies in the PV system and with the same size of synchronous machine replaced
- To evaluate the limit of the generations to be injected in the INPS with respect to stability

1.4 Scope and Limitations

This work will provide the technical impact of the 25MW Nuwakot PV project on the interconnected system of Kathmandu valley. The technical analysis will cover the impact on the voltage and loss on the INPS with and without the PV at Devighat, Nuwakot interconnected to the grid. Moreover, the response on the voltage, power and frequency at the time of the contingencies along with the effect of injection of small disturbances will also be studied. The small signal analysis was performed with the same value of synchronous generation at the same location to determine the impact with the other type of machine. Though the feasibility for the generation of 25MW hydropower has not been done, for the comparison of the effect with the synchronous machine system, the generation is considered to be connected in the same substation as the PV at Nuwakot.

The power factor of the load at substations were assumed to be at 0.9. And the load flow analysis was performed considering a single time load data. The constant PQ load data with constant power has been considered. The photovoltaic and other generations

have been considered as the PQ generation source. Since, the generation source has to maintain the power factor within the limits, thus active as well as the reactive power is being generated from the generating stations, thus is PQ modeled. With the largest generation at the Tamakoshi powerhouse, the generation was considered as infinite grid.

The parameters for the modeling of excitation system and the governor are considered from the models in the Digsilent library and are shown in the Table 1.1 and 1.2 attached herewith.

Table 1.1: Parameters for excitation system

S.N.	Parameters	Value
1	Tr Measurement Delay [s]	0.02
2	Ka Controller Gain [pu]	200
3	Ta Controller Time Constant [s]	0.03
4	Ke Exciter Constant [pu]	1
5	Te Exciter Time Constant [s]	0.2
6	Kf Stabilization Path Gain [pu]	0.05
7	Tf Stabilization Path Time Constant [s]	1.5
8	E1 Saturation Factor 1 [pu]	3.9
9	Se1 Saturation Factor 2 [pu]	0.1
10	E2 Saturation Factor 3 [pu]	5.2
11	Se2 Saturation Factor 4 [pu]	0.5
12	Vrmin Controller Output Minimum [pu]	-10
13	Vrmax Controller Output Maximum [pu]	10

Table 1.2: Parameters for governor

S.N.	Parameters	Value
1	T1 Electric control box T1 [s]	0.2
2	T2 Electric control box T2 [s]	0.1
3	T3 Electric control box T3 [s]	0.5
4	Td Engine delay [s]	0.01
5	PN Prime Mover Rated Power(=0->PN=Pgnn) [MW]	0
6	K Actuator Gain [pu]	15
7	T4 Actuator T4 [s]	1
8	T5 Actuator T5 [s]	0.1
9	T6 Actuator T6 [s]	0.2
10	Tmin Actuator min output [pu]	0
11	Tmax Actuator max output [pu]	1.1

CHAPTER TWO: LITERATURE REVIEW

2.1 Review of Research Papers

Modeling and simulation of the Iraqi 400 kV super grid have been provided in the publication (Al-Akayshee et al., 2020). The model presented in this study and all investigations carried out are regarded as the initial stage in the process of grid assessment for boosting solar generating penetration in Iraq. The load flow research, transient stability scenarios, modal/eigenvalues computation, and short circuit influences on the power system's generating units were also covered in this work. With the help of the simulation tool DIgSILENT PowerFactory, the network was modelled and all results were produced.

In the context of several sites for a synchronous compensator in the grid, the paper (Toma & Gavrilas, 2016) presents a comparison investigation between the impacts on voltage stability of the integration of a wind farm into the electrical grid with or without voltage dependent loads. Power Factory DIgSILENT 15.2.2 and a DPL script that use a simplified version of the Continuation Power Flow method are used to construct the P-V curves.

The paper (Gogoi et al., 2016), load flow simulation studies of the North Eastern Grid of India are investigated using PSS®E, a well-liked and widely-used piece of commercial software from SIEMENS. The system under study consists of 143 buses with various voltage levels and transmission lines that span a distance of 6445 kilometers. For this study, an 80% loading over all lines has been assumed. The model was solved using DIgSILENT, which is also marketed as Power Factory, and the findings were validated by observing a reasonable convergence in both of the results. Various fault types have also been the subject of simulations.

The paper (Abdalla et al., 2012) presents steady-state and transient studies to assess the impact of a 200 MW Central Receiver Solar Power Plant (CRSPP) connection on the Main Interconnected Transmission System (MITS) of Oman. The CRSPP consists mainly of a central solar receiver, power tower, thousands of heliostats, molten salt storage tanks, heat exchangers, steam generator, steam turbine, synchronous generator, and step-up transformer. Two proposed locations are considered to connect the CRSPP plant to MITS: Manah 132 kV and Adam 132/33 kV grid stations. The 2015

transmission grid model has been updated to include the simulation of the proposed 200 MW CRSPP using the DIgSILENT Power Factory professional software. The investigations cover transient reactions to three-phase faults and total CRSPP outages in addition to load flow analysis and short-circuit level predictions. The outcomes have demonstrated that the proposed CRSPP plant's link to the MITS is acceptable.

The paper by (Abdalla et al., 2012) covers steady-state and transient simulations to assess the impact of a 200 MW Central Receiver Solar Power Plant (CRSPP) connection on the Main Interconnected Transmission System (MITS) of Oman. The main elements of the CRSPP include a central solar receiver, a power tower, thousands of heliostats, molten salt storage tanks, heat exchangers, a steam generator, a steam turbine, a synchronous generator, and a step-up transformer. For the link between the CRSPP plant and MITS, consideration is being given to the grid stations Manah 132 kV and Adam 132/33 kV. The 200 MW CRSPP project has been modelled and added to the 2015 transmission grid using the specialized program DIgSILENT Power Factory.

According to this study (Quan et al., 2017) ,distributed photovoltaic (PV) generation has an impact on grid voltage, network power loss, and the loading of network elements. This study also provides a quantitative expression of penetration. Additionally, it examines the test grid's maximum PV capacity that is accessible and suggests the essential location of high penetration. The effects of highly embedded distributed PV generation on grid voltage, network power loss, and network element loading are then examined using continuous load flow calculations.

An overview of inertia's function in the developing power system is given in this manual(Denholm et al., 2020). It explains the causes of inertia in the grid, how it interacts naturally with other grid services, how much inertia is needed, what influences these needs, and what adjustments may be made to preserve reliability as it deteriorates. It is aimed for audiences who are not technically savvy. Additionally, it presents understandable examples to clarify the ideas of inertia and other grid services that are necessary to preserve system frequency, which is a crucial sign of grid health at the moment. The guide also covers alternatives to conventional inertia and offers a number of key insights that decision-makers, planners, operators, analysts, and other stakeholders in the power system may find useful.

If energy-constrained units are permitted to engage in the ancillary service markets, this research(Borsche et al., 2014) explores many elements and potential benefits for power system operation and stability. Primary frequency response is one additional service that batteries can offer. However, they have a finite amount of energy. Set-point adjustments are therefore required, and the energy for them must still be delivered by power plants that are not constrained by energy.

In this study (Ulbig et al., 2015) , the impact of various grid topology configurations and low rotational inertia on the stability of a three-area power system is examined. The submitted contributions expand on earlier findings for a two-area power system using analytical and simulation-based insights. This study(Ulbig et al., 2014) explores the effects of low rotational inertia on the operation and stability of power systems, offers new analysis insights, and suggests ways to mitigate the effects.

The goal of this study(Johnson et al., 2019) was to identify the conditions under which an electric grid would be more susceptible to frequency contingencies, such as a generator outage. System inertia, a recognized proxy for grid stability, was measured using unit commitment and dispatch modeling. To demonstrate the approach, a case study of the Texas Electric Reliability Council grid was employed. The outcomes of the modeled scenarios demonstrated that the Texas grid is resilient to significant system changes, even with very high penetrations of renewable energy (30% of annual energy generation compared to 18% in 2017). However, the model's retirement of nuclear power facilities and its inclusion of private-use networks resulted in unstable inertia levels in our findings. Multiple coal and natural gas combined-cycle plants were dispatched at part-load or at their minimal operating level to ensure stable system inertia levels when the system inertia was constrained in our model to reach a minimum threshold. This behavior could occur on other electric grids that depend on synchronous generators for inertia support, and it is predicted that it will increase with larger penetrations of inertia-less renewable energy.

2.2 Transient Stability (Voltage, Frequency and Power)

The ability of the power system to sustain synchronism in the presence of a significant transient disruption, such as a breakdown on transmission infrastructure, a loss of generation, or a loss of a sizable load, is known as transient stability. Large deviations in generator rotor angles, power flows, bus voltages, and other system variables are

among the effects of these disruptions. If the resulting angle between the machines in the system stays within the limit, the system is still in synchronism. If temporary instability causes a loss of synchronism, it will typically become apparent within 2 to 3 seconds of the disturbance. The PV and generator outage conditions are taken into account for the transient analysis.

Also, the stability of a system during and after abrupt changes or disturbances, such as short circuits, generator failure, sudden changes in load, line tripping, or any other impact of a like nature, are referred to as transient or dynamic stability. When all synchronous machines return to their steady-state operating condition after a significant disruption without experiencing a protracted loss of synchronism or falling behind other machines, the system is said to be transiently stable. Any synchronous machine's transient stability limit is a power angle of less than 180 degrees.

A power system's capacity to maintain electromechanical balance under both typical and unusual operating situations is known as power system stability.

The ability of designated synchronous machines to maintain synchronism with one another after disturbances like faults and fault removal at different points in the system is how the power system stability is characterized because it is an electromechanical phenomenon. Additionally, it shows how well the system's induction motors can continue to generate torque after these disruptions in order to bear load.

The design and operation of a power system depend heavily on its dynamic performance. The machine power angles and speed deviations, the system electrical frequency, the real and reactive power flows of the machines, the power flows of the lines and transformers, as well as the voltage levels of the buses in the system, are all determined by the transient stability research. These system conditions offer clues for evaluating the stability of the system. The one-line diagram shows the findings, which can also be printed or plotted. The modeling of specific machine groups in the system, which are known to have significant effects on the system's operation, is necessary for transient stability investigations. For each research example, the total simulation period should be sufficient to draw a firm conclusion about stability.

The following are just a few of the main causes of industrial power system instability:

- Short-circuits
- Loss of an in-plant cogeneration component;
- Loss of a tie connection to a utility system (generator rejection)
- Impact loading (motors and static loads),
- switching operations of lines, capacitors, etc.,
- Starting a motor that is huge compared to the system's generating capacity, impact loading (motors and static loads), and
- a rapid large step change in load or generation

The effects of power system instability issues are typically highly severe and can range from shutting down operations and permanently damaging equipment to causing a complete area to lose electricity. The following is a list of typical effects:

- Area-wide blackout
- Load interruption
- Low-voltage circumstances
- Equipment damage
- Relay and protective device malfunctions

2.3 Small Signal Stability

Two alternative solar photovoltaic generating models that are appropriate for small signal stability analysis are described in this study (Parmar & Mehta, 2018) , and their behavior is examined while taking the IEEE 14-bus test system into consideration. The study examines how the control of active and reactive power production affects the effects of solar energy on an interconnected power system that has a high penetration of PV generation. The impact of voltage and angle stability on grid-connected PV systems is investigated and addressed using models with constant reactive power and constant voltage magnitude. The power system analysis toolbox on the MATLAB platform is used to perform the eigenvalue analysis for the test system with and without PV penetration at various levels, and the results are compared. The essential modes that have the biggest impact are determined, and their behavior as PV penetration increases is shown.

With the aid of Lyapunov's stability criteria, this research (Sadhana et al., 2017) analyzes the procedure used in the stability studies of an integrated hybrid power system. For many renewable energy sources, such as wind generation systems, solar PV systems, and micro hydro systems, stability assessments can be carried out. This study examines a wind generation system that is connected to the four-machine Western System Coordinating Council (WSCC) system. The focus of the stability analysis is on the various operational states of the WSCC four-machine system with random values for generation and demand. MATLAB/Simulink is used to conduct simulation studies on the WSCC four machine system in order to assess stability. The Monte Carlo Approach is used to validate this study for iteration-based evaluations. This study demonstrates the important benefit of doing stability studies with uncertainty constraints involved, as opposed to deterministic stability studies, such as possible transfer capability restrictions to cancel out inadequately damped oscillations from power system operation.

The influence of large-scale PV power plants on a transmission system is examined in this study (Remon et al., 2017) for various penetration levels. The analysis compares the performance of synchronous power controllers (SPCs), which enable power converters formed into power plants to interact harmoniously with the grid, to that of traditional power converter controllers, assuming that the power plants participate in frequency and voltage regulation in both cases. The study deals with the system's response to significant disturbances that change the active power balance and frequency stability as well as the small-signal stability of the system. The analysis's findings demonstrate that PV power plants using SPCs can minimize stress on other producing units, increase oscillation damping, and limit frequency deviations, all of which have a positive effect on the power system.

The approaches used to ensure the rotor angle stability of electric power systems—which is most typically studied with small-signal models—are the main topic of this research (Nikolaev et al., 2021). The major tools for enhancing the small-signal stability of electromechanical oscillatory modes over the past few decades have been power system stabilizers (PSSs) for conventional excitation systems.

Both PV and different Flexible AC Transmission system (FACTS) devices have been introduced to a standard two area system in this work (Srivastava et al., 2018) for

stability investigations. This was accomplished by contrasting the damping provided by various FACTS devices and PV. Time domain simulations are used to conduct the thorough analysis. In-depth discussion is also given to both the voltage profile and steady state stability. The PSAT toolbox of MATLAB was used to perform all simulations and analysis.

Key characteristics of the eigenvalues of linearized system in regard to stability are:

- The system is said to be asymptotically stable if all of the eigenvalues have negative real parts, which means that after a brief disturbance, the system resumes its stable state.
- If one of the eigenvalues has a positive real part, the system is unstable as it can not return to its initial position after a disturbance.
- If the system contains all the eigenvalues with negative real part but one with purely imaginary portion, then the system demonstrates oscillatory behavior; dubbed critically stable or marginally stable.

One or two zero eigenvalues can be found in the majority of research or commercial analysis development tools for eigenvalue analysis. The reason for those zero eigenvalues is that if all machine angles are held (not changed), there is no infinite bus in the system for the reference angle. Machines in the system might continue to synchronize at a speed other than the initial synchronous speed. According to traditional power system stability, this is considered stable. The absence of turbine governor control model can also lead to eigenvalues of zero. In this study, eigenvalues have been determined together with damping ratio and frequency of oscillation for different instances.

CHAPTER THREE: METHODOLOGY

3.1 Block Diagram

The methodology followed during the course of thesis is presented in Figure 3.1.

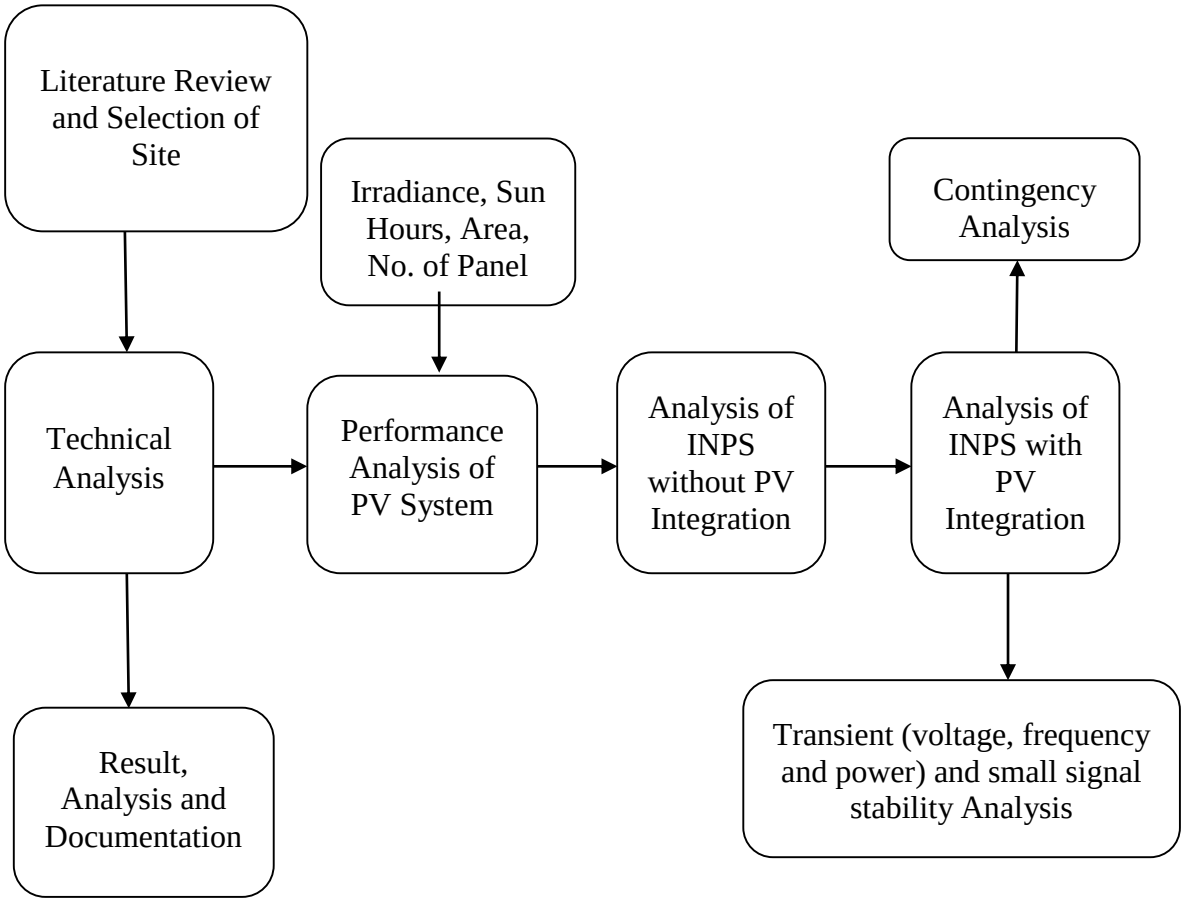

Figure 3.1: Overall block diagram methodology

3.2 Collection of Data

The data required for the study is collected from numerous sources. The major data sources include the NEA Annual Book and Transmission/Project Management Directorate Annual Book of FY 2077/78. During the modeling of the system the Single Line Diagram (SLD), the reference for substation connections, conductor size and configuration, Hydropower Plant (HP) connection and generation capacity is considered from the INPS layout available in those publications. The load data is reflected from the data provided from the various Grid Divisions/Branches. For the

analysis, the both the generation and load data are considered from the month of Bhadra of year 2078.

3.3 Performance analysis of the System

The simulation of the Nuwakot PV is performed for the determination of annual performance along with the annual energy yield to the grid. This analysis has been performed in the PVSyst software. For the grid connected system, the meteo database for the site at Nuwakot is taken along with the PV panel and inverter system. In the PVSyst the generation capacity is provided for the PV system, with the hourly sun data available from the Metronorm 8.0 data (a sample of the monthly values are provided in Figure A.2), the efficiency, energy generation and daily generation outputs are then computed as the results of the PV system.S

3.4 System Modeling

The INPS is simulated in the DIgSILENT 15.1.7 software. In the modeling of the INPS, the load model the constant kVA load is assumed. The power factor of the load is assumed to be 0.9 (average pf of each SS). The transmission line parameters are computed as per the conductor reference provided in the IS 398-1976 standard. The generation at the Tamakoshi PH is considered as the infinite bus importing being the highest source of generation. For the PV and DG generation, the simulation models in the DIgSILENT are considered.

3.5 Load Flow Analysis

The Load Flow Analysis (LFA) in the DIgSILENT is performed using Newton-Raphson method. This method presents a smaller set of steps for iterations until a possible condition of divergence is met. Those set of minor rises in the values can help to meet a solution of the load flow in case of some of the systems where the failure of the other method might have occurred. According to the test results, the approach can enhance convergence for distribution and transmission systems by having considerable series capacitance effects (i.e., negative series reactance).

The power flow analysis is to be performed to find the voltage profile and the overall loss of the existing system and the after the injection of the PV. The following load flow equation is used and iteratively solved using the Newton-Raphson method.:

$$\begin{bmatrix}\Delta P\\ \Delta Q\end{bmatrix} = \begin{bmatrix}J1 & J2\\ J3 & J4\end{bmatrix}\begin{bmatrix}\Delta\delta\\ \Delta V\end{bmatrix} \quad \ldots\ldots \quad (3.1)$$

where ΔP and ΔQ stand for the real power and reactive power mismatch vectors on the bus, respectively; ΔV and $\Delta\delta$ stand for the incremental bus voltage magnitude and angle vectors; and J1 through J4 are referred to as Jacobian matrices.

The Newton-Raphson approach has a special quadratic convergence property. Compared to other load flow computation techniques, it often has a very fast convergence speed. The fact that the convergence criteria are predetermined to guarantee convergence for bus real power and reactive power imbalances is another advantage. You have complete control over the level of precision you want to specify for the load flow solution thanks to this criterion. The Newton-Raphson method's convergence criterion is commonly set at 0.001 MW and Mvar.

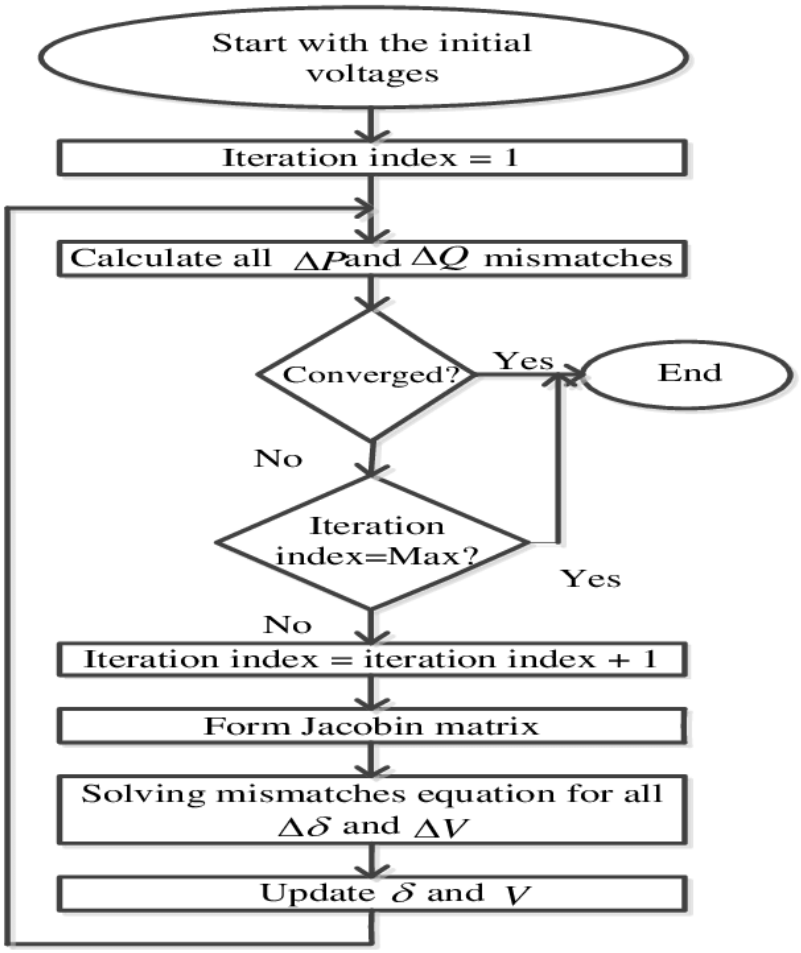

Figure 3.2: Newton-Raphson methodology of load flow

System Regulations on Voltage, power factor and Loading

The voltage and loading of the overall system were studied and conformed to the NEA Grid code. As per this, the bus voltages at all the system connections should be within the limit of 95% and 105% under the normal operating condition and between 90% and 110% for the Grid system under alert condition. Thus, the voltage at the system should be maintained in range 5% to 10% of the nominal value to avoid collapse in voltage and shutdown of the consumer loads.

The generation shall be capable of supplying varying reactive power support to maintain power factor within the leading value of 0.95 and 0.85 lagging.

Also, the loading of all the transmission lines and substations should be below 90% of their continuous ratings. The transmission lines across the interconnection shall have same characteristics in terms of capacity and thermal capacity to avoid loading issues.

3.6 Transient Analysis Tool

The response of the system for the varying generations on the bus voltage, system frequency and power generations on the nearby system was studied. With the use of a simulation scan function, the RMS simulation tool in DIgSILENT PowerFactory may be used to examine mid- and long-term transients under balanced and unbalanced circumstances. Model definition is done using the DIgSILENT Simulation Language (DSL), and there is a sizable library of IEEE standard models accessible. The standard models for the generator incorporating the governor and excitation system are placed from the standard library with the parameters as provided in tables in subsection 1.4 and simulation models in Figure 4.2.

With the PV system at Nuwakot, the transient analysis was performed with the replacement of the same size of synchronous generation considered. The models and the parameters for the simulation system considered for the additional PV and synchronous machine added to the system was shown in Chapter one.

System Regulation on Frequency

The system frequency should be maintained within the limits of 49.5Hz and 50.5Hz under the normal operating conditions. Under the alert conditions the frequency is limited within the limits of 48.75Hz and 51.25Hz.

3.7 Small signal stability analysis

A collection of n first-order nonlinear differential equations and a set of algebraic equations can be used to describe the behavior of a dynamic system, such as a power system.

$$\dot{x}_i = f_i(x, y, l, p)$$
$$O = g_i(x, y, l, p) \quad \ldots\ldots \quad (3.2)$$

If l and p are uncontrolled and controllable parameters, respectively, and x is a vector of state variables, y is a vector of algebraic variables. The preceding set of equations can be linearized to investigate the system oscillatory behavior because the disturbance considered here is minimal. Thus, the linearized system can be expressed as follows:

$$\Delta\dot{x} = A\Delta x + B\Delta u$$
$$\Delta y = C\Delta x + D\Delta u \quad \ldots\ldots \quad (3.3)$$

The state matrix A's eigenvalues indicate the linearized system's stability, and the right eigenvector (φ) and left eigenvector (ψ) determine the participation of each system state in a given eigenvalue. The following definitions apply to the system matrix A's i^{th} eigenvalue and its associated eigenvectors:

$$A\Phi i = \lambda i \Phi i$$
$$\Psi i A = \lambda i \Psi i, \quad \ldots\ldots \quad (3.4)$$

The mode frequency in Hz (f) and the damping ratio (ς) are expressed as follows for a complex eigenvalue that represents an oscillatory mode of the system:

$$\lambda i = \sigma_i + j\omega_i$$
$$f_i = \frac{\omega_i}{2\pi}$$
$$\zeta i = \frac{\sigma_i}{\sqrt{\sigma_i^2 + \omega_i^2}} \quad \ldots\ldots \quad (3.4)$$

Damping ratio, which is connected to the real component of the eigen value's controls how quickly the oscillations' amplitude decrease.

Calculation Method:

There are two possible calculation methods for the Modal Analysis, they are:

- QR/QZ-Method; This method is the 'classical' method for calculating all of the system eigenvalues.
- Selective Modal Analysis (Arnoldi/Lanczos); This method only calculates a subset of the system eigenvalues around a particular reference point. Often this method is used in very large systems when using the QR-method could be very time consuming. It is especially useful if the user knows the target area of interest for the eigenvalues. This option needs more configuration as explained below.

In this study QR/QZ-Method has been used since all the eigen values were needed to be evaluated for the system analysis, while the other method calculates only a subset of eigen values around the reference point provided and is relatively slow than the QR/QZ-Method.

With the PV system at Nuwakot, the small signal stability analysis was performed with the replacement of the same size of synchronous generation assumed. A disturbance of 0.01pu has been injected at the hydropower generation at Devighat and the effect on the system was analyzed.

CHAPTER FOUR: RESULTS AND DISCUSSIONS

4.1 Energy and Loss on PV system

The simulation of the PV is performed to determine the overall performance of the 25MW PV power plant. The result as shown in Figure 4.1 indicate that the annual production of the PV system is 80.8% of the system installed capacity varying in between 78% to 86%.

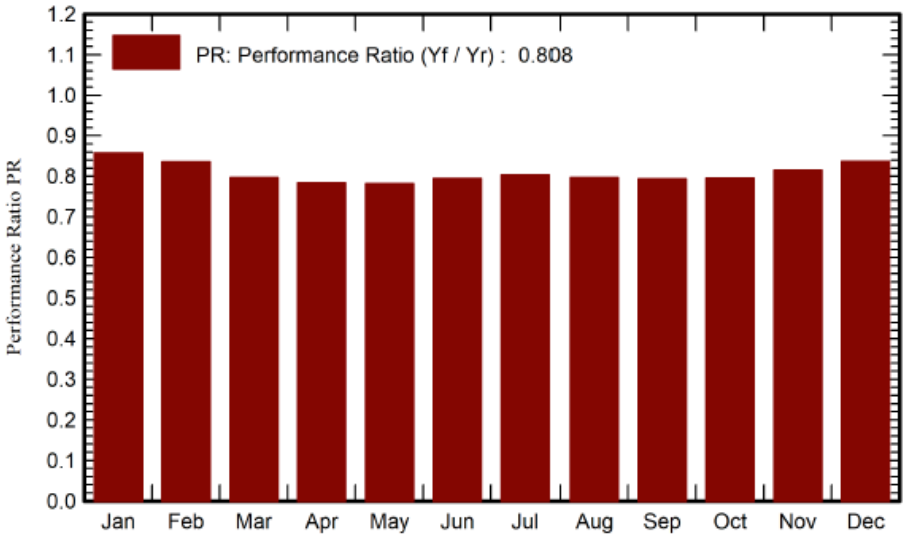

Figure 4.1: Performance Ratio (PR) of the Nuwakot PV System

Similarly, the normalized production of the solar power plant is 4.52kWh/kW/day as presented in Figure 4.2. And the system suffers a loss of 0.99kWh/kW/day in collector and 0.09kWh/kW/day in inverter system.

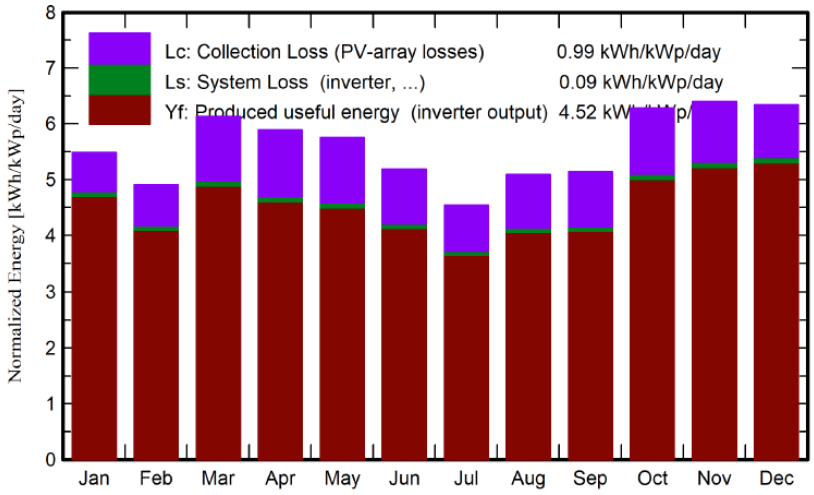

Figure 4.2: Normalized production of the solar system kWh/kW/day

The simulation yielded the daily system energy which can be injected in the grid for the annual time period. The system can generate up to 153MWh/day energy and in any cloudy day can fall down below 19MWh as shown in Figure 4.3. In average the system can generate an energy about 113MWh energy and 41.2GWh annually.

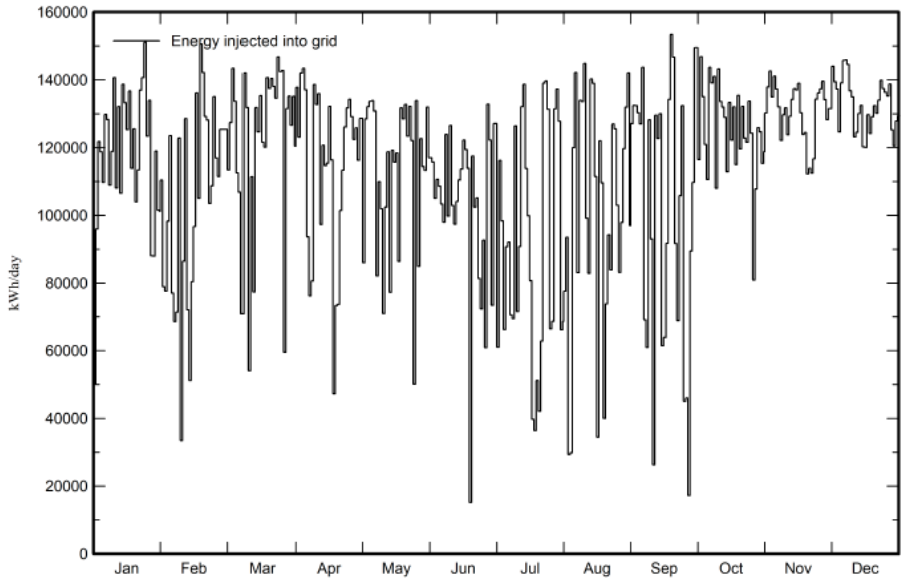

Figure 4.3: Daily energy production by PV at Nuwakot

The histogram of the daily power injected into grid is shown in Figure 4.4. This represents that maximum generation reaches to 18MW at certain days. The loss diagram of the overall 25MW PV system at Nuwakot is presented in Figure 4.5.

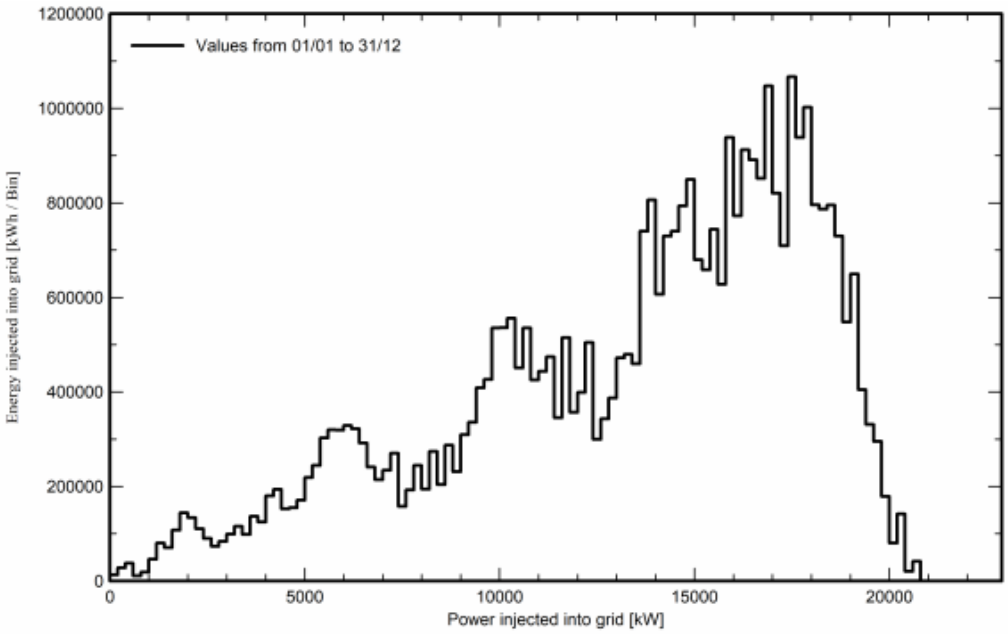

Figure 4.4: System output power distribution for Nuwakot PV

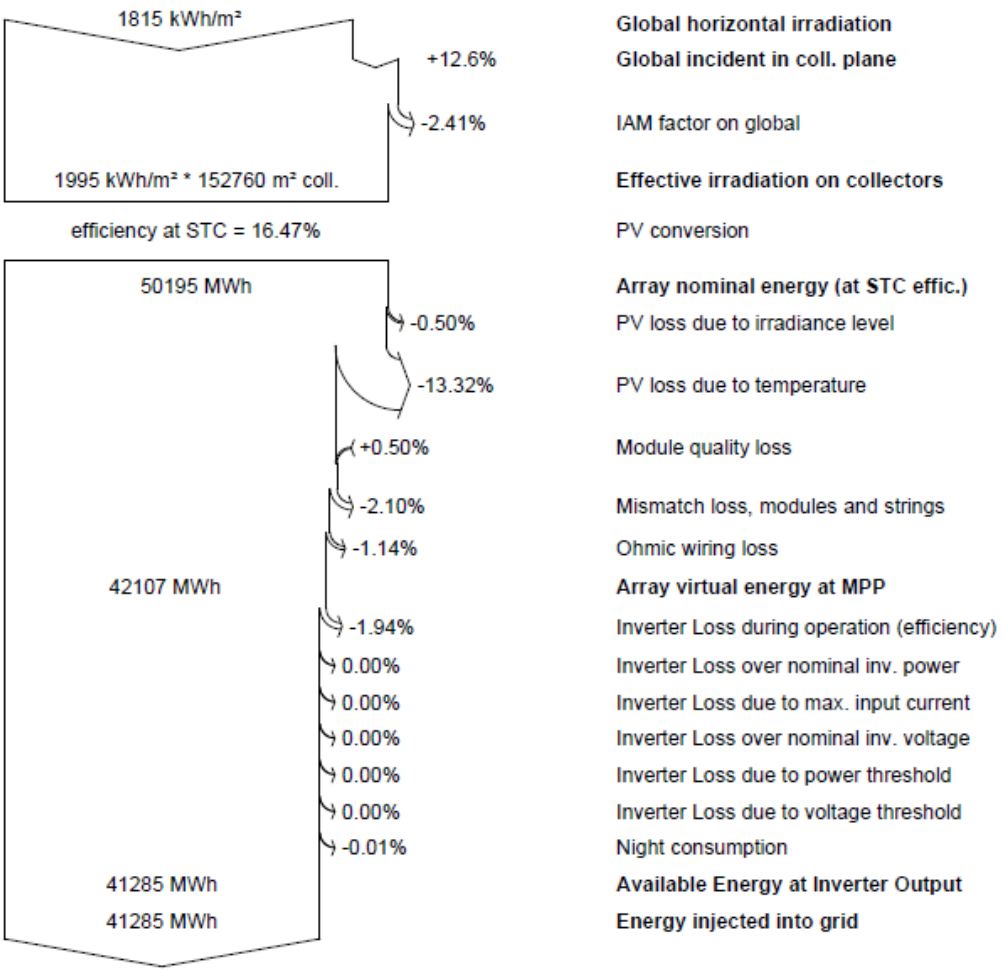

Figure 4.5: Loss diagram of the PV system

4.2 Simulation Model

The PV and the synchronous machine for the simulation is considered from the available models in DIgSILENT. For the PV generation a simple model with constant PQ was considered as mentioned in the previous sections. For the synchronous machine overall system of Generator and Turbine, excitation system and synchronous machine model was combined as shown in Figure 4.6. The overall frame incapsulates these systems and is shown in Figure 4.7.

The parameters of the excitation system and governor and turbine was as per the Table 1.1. and Table 1.2 previously illustrated.

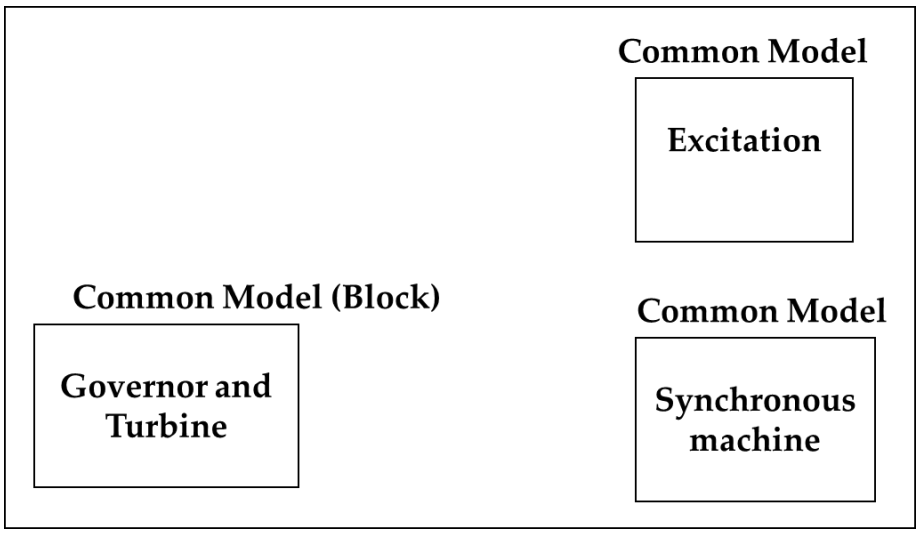

Figure 4.6: Overall model for synchronous machine

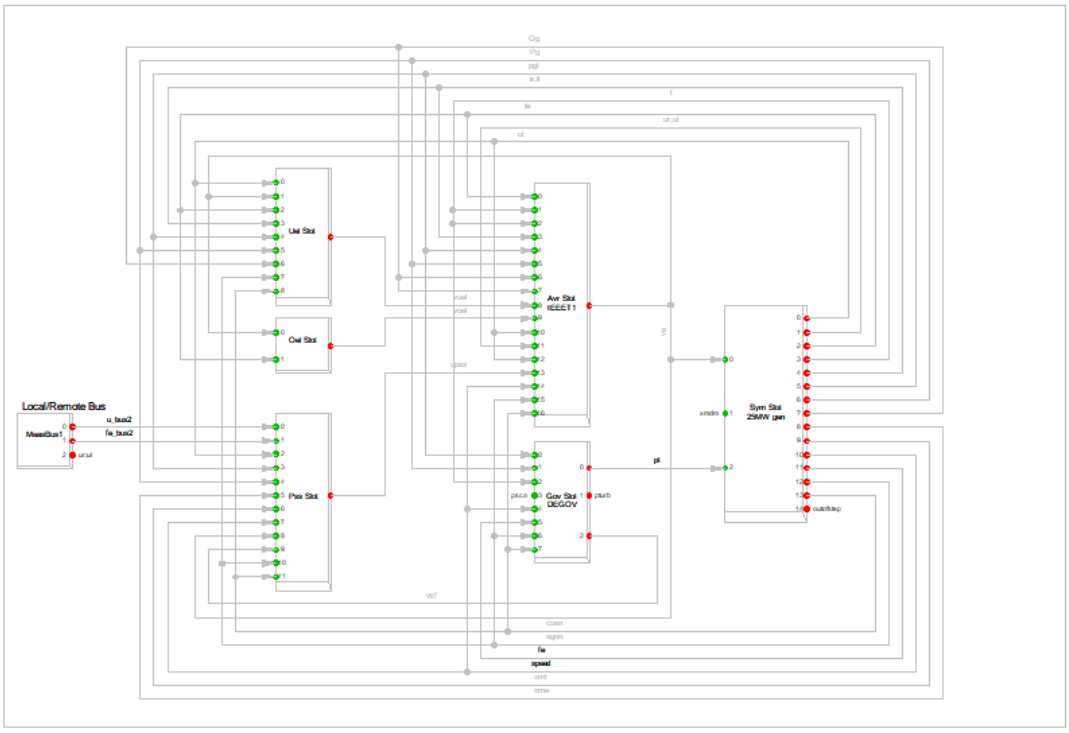

Figure 4.7: Model of frame for synchronous machine

The excitation system model considered for the synchronous machine is shown in Figure 4.8. IEEET1 model of the excitation system is used with the parameters as in subsection 1.4. Also, the model of the governor for synchronous machine is presented in Figure 4.9.

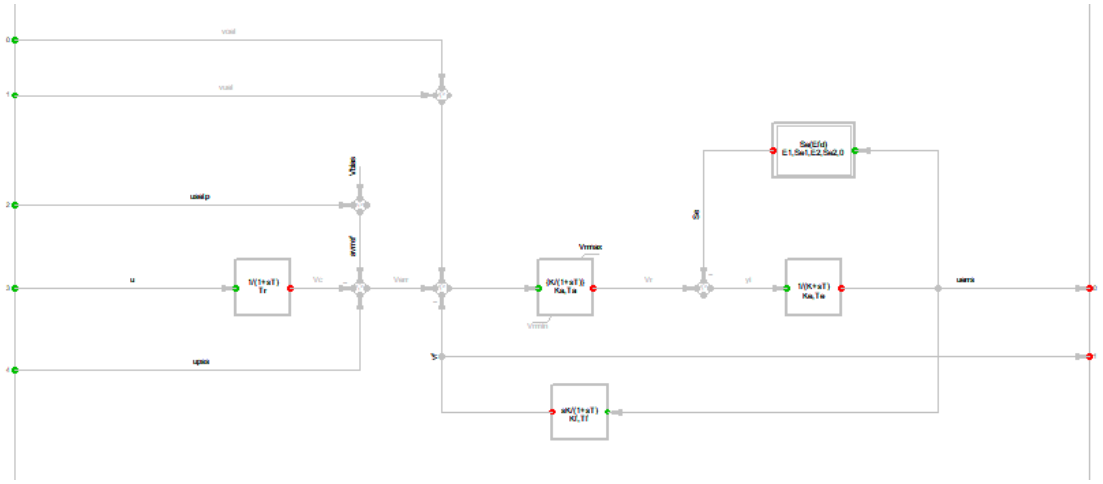

Figure 4.8: Excitation system for synchronous machine

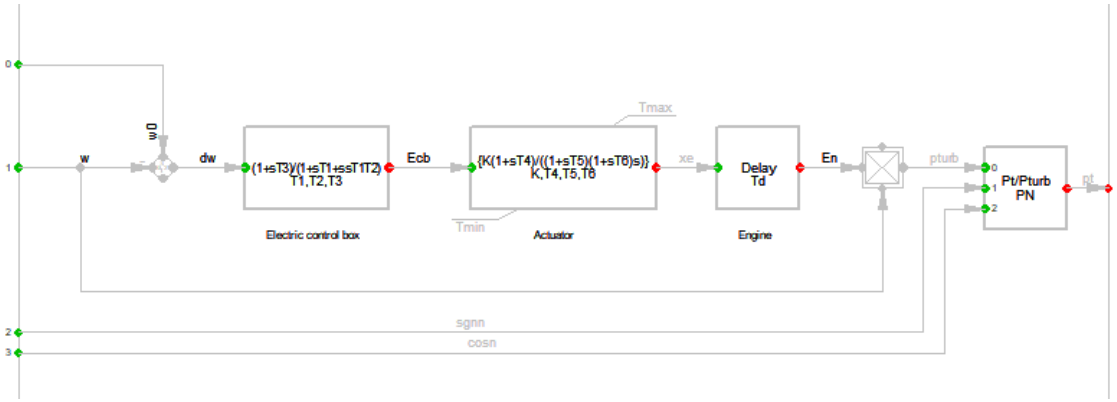

Figure 4.9: Governor for synchronous machine

4.3 Analysis of Existing INPS System without Nuwakot PV

The existing interconnected system of INPS within the Kathmandu valley is simulated considering the peak loading conditions. The existing system without the PV connected at Devighat substation is analyzed. From the simulation, the voltage and loss results of the system is evaluated. The generation through Tamakoshi power house Grid was considered as the infinite grid for the simulation purpose as it is the greatest source of generation.

The Figure 4.10 illustrates the nodal voltage at the various substations. From the analysis it was determined that the minimum voltage at the higher system loadings occurs at Lainchaur substation located in Kathmandu valley province which is i.e., 0.969pu, which is still in the limits of ±10% as per electricity regulation guidelines.

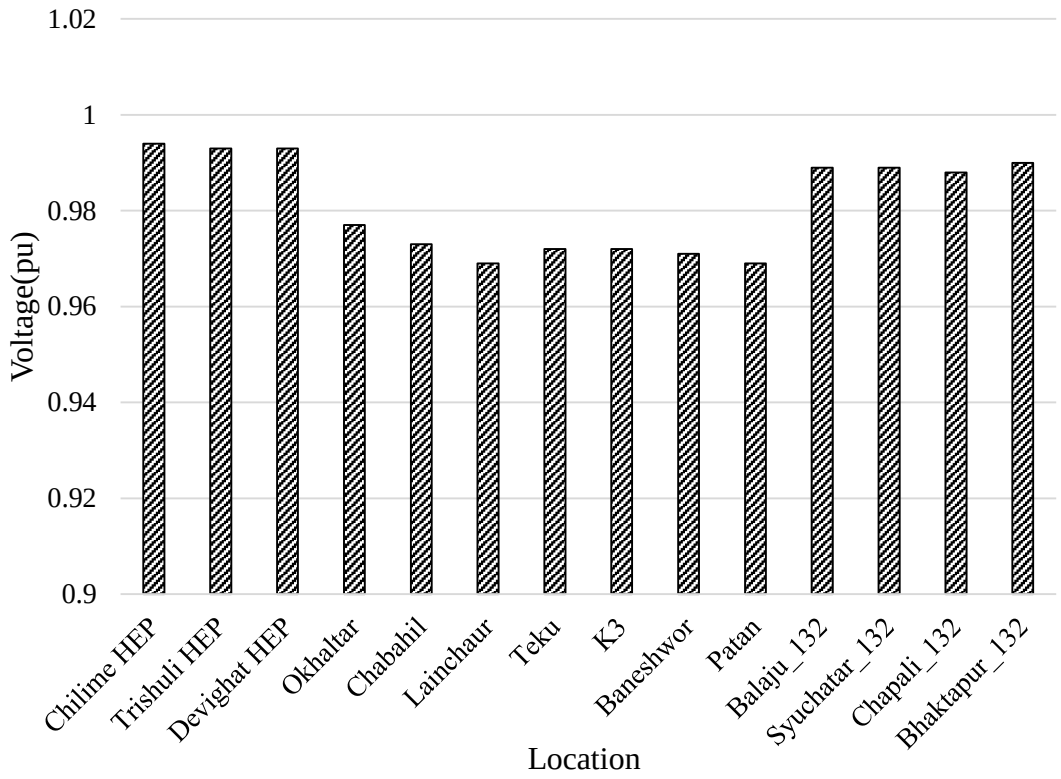

Figure 4.10: Nodal voltages at 132/66kV substations/generations

The existing 132/66kV transmission system suffers an overall loss of 8.4MW at the peak loading conditions which is equivalent to 3.47% of the overall dispatched load.

4.4 Analysis of System with PV plant at Nuwakot

The 25MW substation is connected to the INPS with Devighat substation as the connection point. The result yielded improved voltage profile of the substation with the major impact in the substations located at Kathmandu valley.

The voltage at the 132/66kV substations is shown in Figure 4.11. As mentioned, with the placement of the 25MW PV system at Nuwakot, the voltage of the nearby substation increases significantly while the others at distant was negligibly affected. It was similar in case of the 66kV substations as well.

However, with the PV connected to the existing system, the 132/66kV loss increases from 8.4MW at peak to 9.98MW i.e., to 3.96%. Though with this generation, the voltage at the nearby substations is improved and the loss decreases in those line sections, but as the power needs to be transmitted either to the Balaju substation with the double circuit (DC) Dog/ and single circuit (SC) Wolf conductor of about 35km

length or to the Chapali substation at 29km length of DC Dog and underground cable, the loss would be higher.

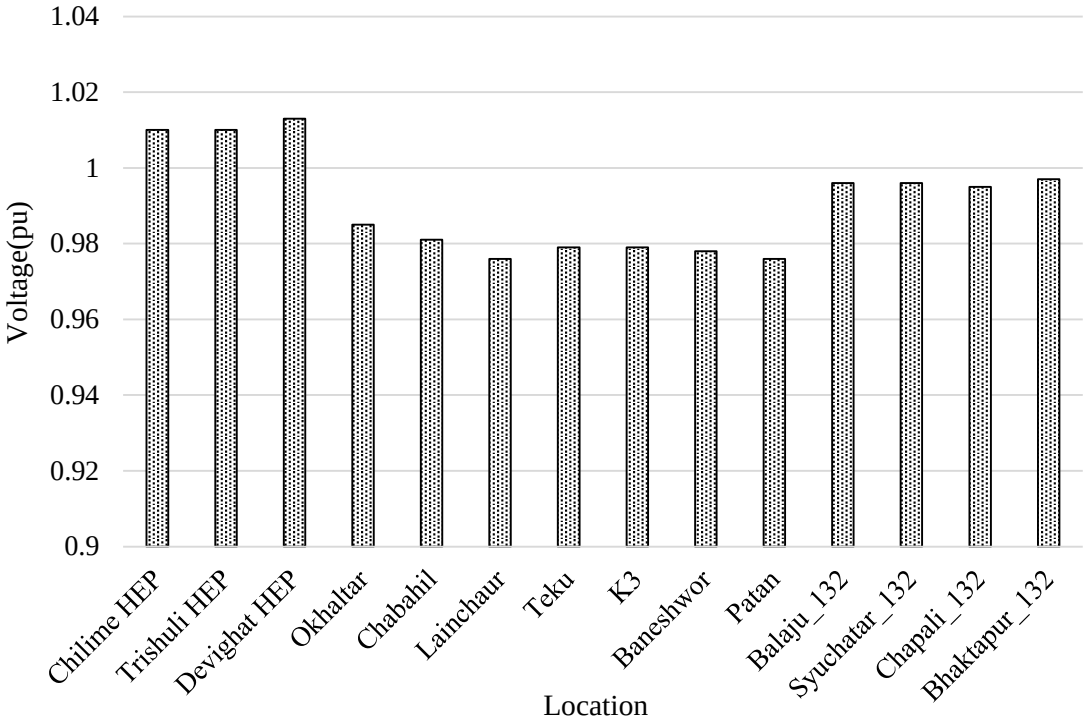

Figure 4.11: Nodal voltages at 132/66kV substations/generations with Nuwakot PV integration

The comparison of the voltage variation in the INPS system before and after the interconnection of the Nuwakot PV is shown in Figure 4.12.

The generation capacity of the PV is increased to check the limit at which the loading or voltage limits are violated. Table 4.1 presents the different generation values obtained through hit and trial and those conditions are checked.

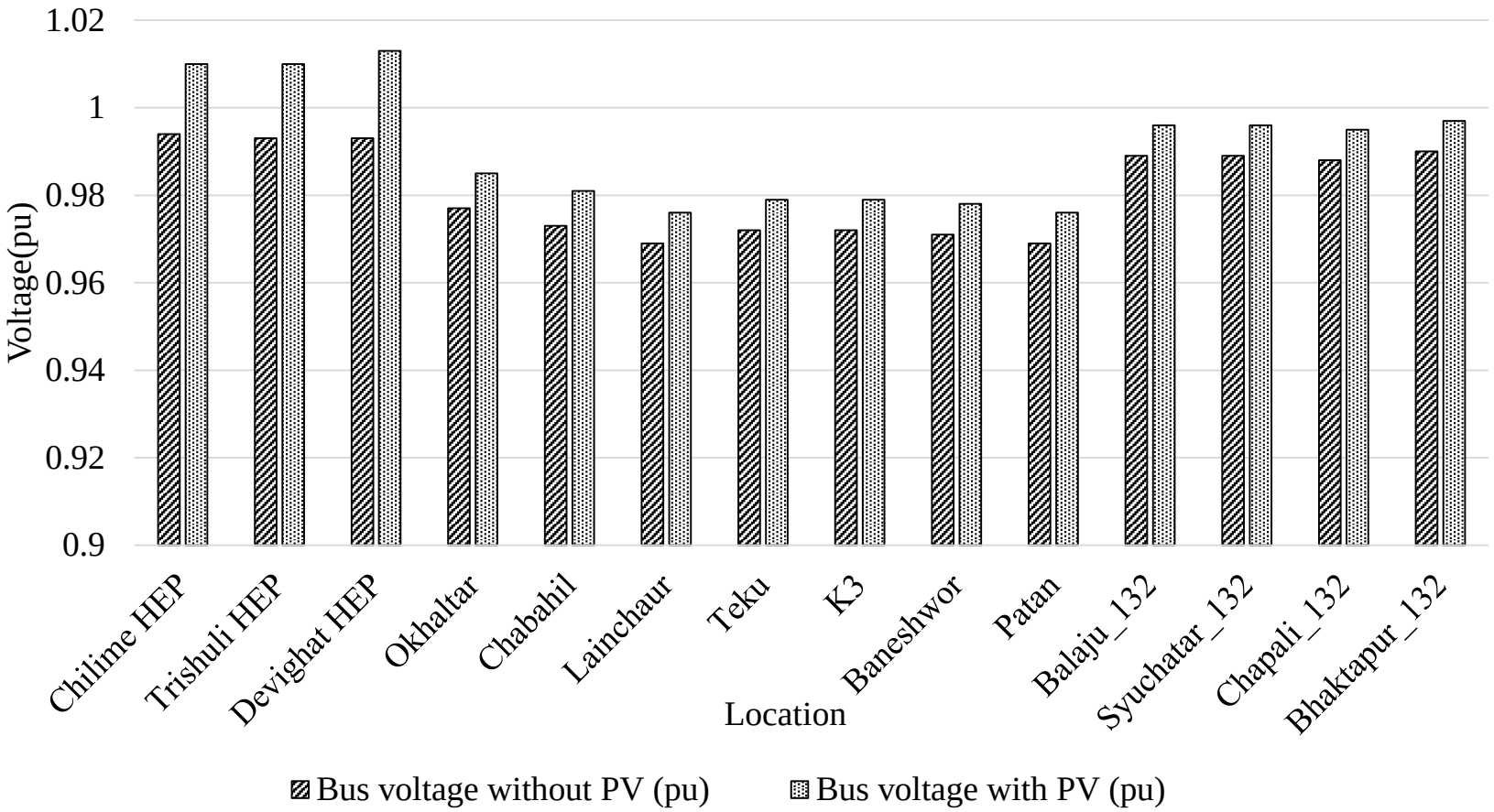

Figure 4.12: Substations voltages before and after PV integration

Table 4.1: Bus voltage and line loadings at various generation values

Generation (MW)	0	25	46	73
Bus Voltage Devighat Station(pu)	0.99	1.005	1.012	1.020
Line Loading (Devighat to PV station) (%)	0	55.1	100.4	157.6
Line Loading (Devighat to Trishuli) (%)	29.8	22.4	31.8	100.5
Line Loading (Devighat to Okhaltar) (%)	39.3	60.6	78.2	51.8

From the Table 4.1 it can be seen that the generation beyond 46MW would cause an overloading of the line in between Nuwakot PV station and Devighat substation, with a significant increase in the bus voltages. As the generation exceeds 73MW, the line from Devighat to Trishuli substation would also get overloaded. So, for the Nuwakot PV, the magnitude of the generation cannot be increased above 46MW for all the line loading to be below 100% loading.

4.5 Transient Response on Isolation for Photovoltaic system

The response of the PV system when it suddenly isolates from the INPS is studied. It was considered at the time t=10 seconds, the PV isolates from the grid. For the inertia-less system 25MW PV generation, the voltage at the terminal of the PV power plant is shown in Figure 4.13.

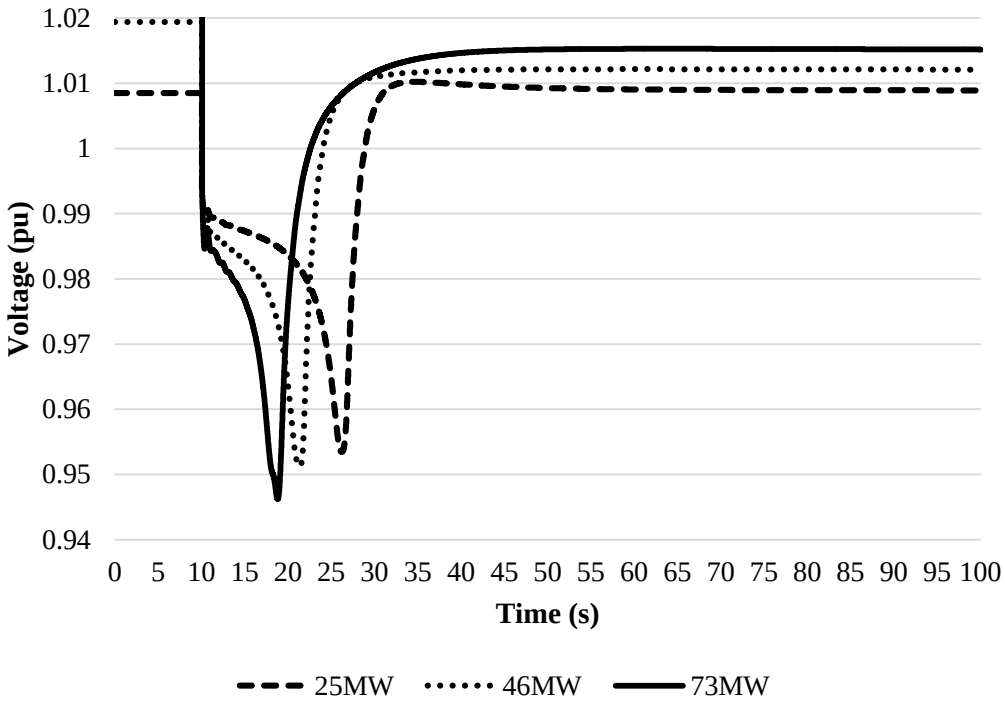

Figure 4.13: Transient response of voltage at Devighat substation for photovoltaic system at various generations

From the figure it can be inferred that, when the PV suddenly isolates from the INPS, the voltage of the terminal bus drops down to 0.954pu from existing 1.008pu. This drop was sudden for a very small amount of time and then decreases gradually and due to the inertia of the system again decreases rapidly to the minimum point. Then after there was a sudden increase in the terminal voltage and reaches to 1.01pu, higher than that of the previous value and then the system slowly stabilizes near to its previous value after about 50 seconds.

The result was a bit different for 46MW system. The initial voltage of the system was about 1.02pu, comparatively higher than the previous due to the higher generation. When the PV system isolates the voltage change follows the similar pattern, however is quickly stabilized than the previous case, after about 38 seconds.

Similarly, the simulation is also carried out with 73MW system. As in the system with 46MW generation, the initial bus voltage is higher than that after the stabilization when the PV system is disconnected from INPS. This system slowly stabilized after about 46 seconds. The terminal bus voltage with respect to the time is compared in Figure 4.13.

So, from the analysis it has been observed that for the inertia less system, with the generation increasing higher than a certain limit the stabilization time increases and there would be a severe voltage drop in the system following the disconnection. The response pattern would be similar in all of the cases of PV isolation, with minor variation in the attributes of voltage and stabilization time.

4.6 Transient Response on Isolation for Synchronous Machine

The similar transient analysis is performed considering the synchronous machine in place of the PV generation for the same magnitude of generation. The transient nature on the voltage was similar to the previous case for the PV system. However, for the synchronous system, the minimum voltage reached in the transient period would be higher than that for the case with PV, as the machine generates some reactive power with the active generation. After certain time interval, the stable condition is reached in which the voltage in the terminal bus was found higher than the previous case. Because with the generation occurring, the generation was tried to be made at the voltage near 1pu.

The response was also obtained for 46MW generation as in Figure 4.14. The transient effect seen due to this generation differs drastically from the previous conditions. The voltage does not decrease by a huge margin as compared to the previous ones. Similarly, the response for the 73MW, as compared to the previous 46MW generator, the voltage stabilizes quicker for this system.

In case of the synchronous system, with the increase in the generation voltage, for certain generation limits, the stabilization time reduces and the transient response would be gradual.

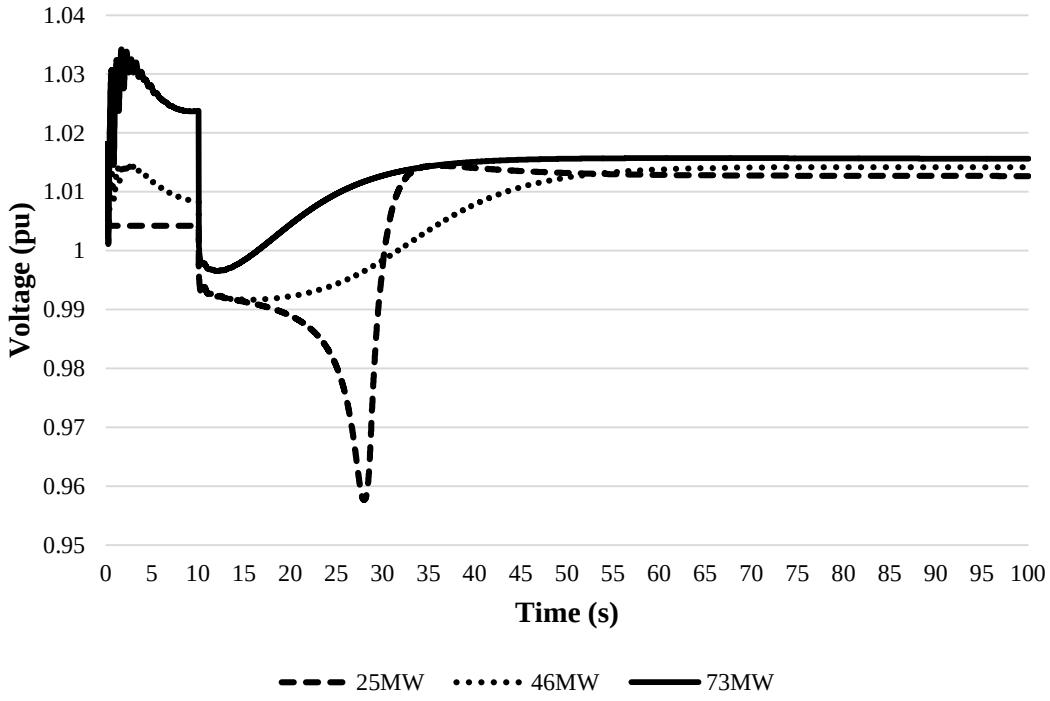

Figure 4.14: Transient response of voltage at Devighat substation for synchronous machine at various level of generations

4.7 Transient Response with Contingency Scenario

A scenario has been considered that the generation at Trishuli PH turns off after 2 seconds and the effect has been analyzed for the 25MW photovoltaic system and for the same rating of synchronous machine system replaced with the existing PV system. The transient response observed in the Devighat substation and power house are illustrated in terms of the voltage, frequency and power generation herewith. The frequency response for the synchronous machine at Devighat hydropower represents the overall frequency response of the interconnected substations and generation inside

the Kathmandu valley. The comparisons are made at various generation levels. The voltage at the Devighat substation and the power and the frequency of the hydropower at the Devighat powerhouse were studied and presented in the following cases.

Case I: At 20% of generation

Figure 4.15 shows that transient drop in the voltage is similar for the generation values of PV and the synchronous generator. The response of the system is much quicker for the synchronous generator, the minimum transient voltage is reached faster and also, the transient value settles quicker for synchronous generator. The minimum voltage reached was about 0.957pu which is within the acceptable limits of the system

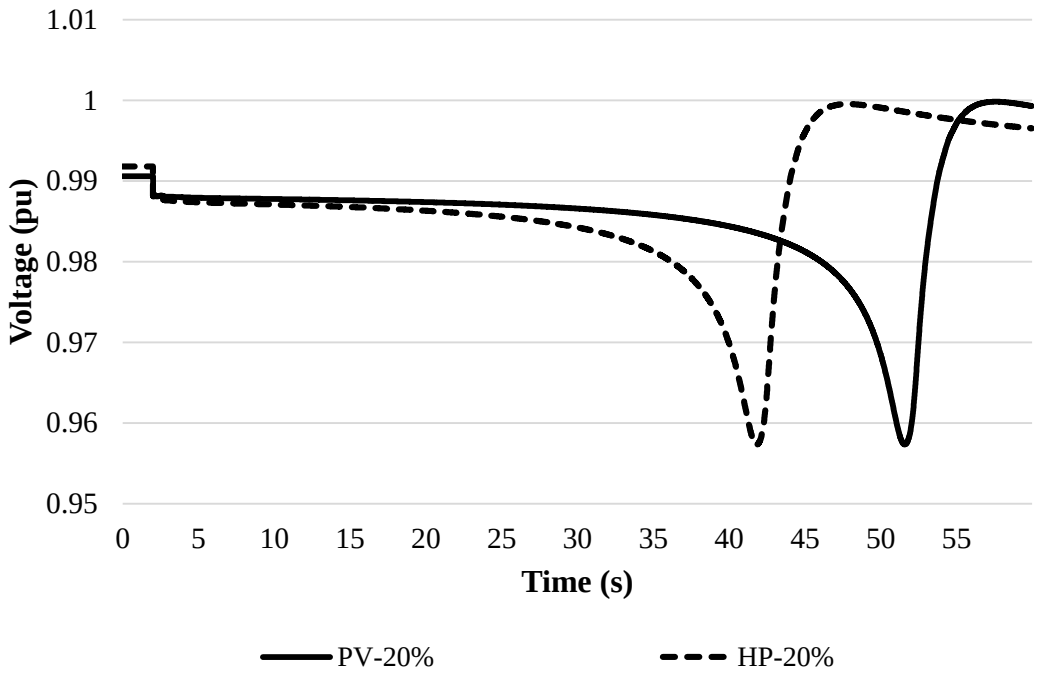

Figure 4.15: Voltage response on Devighat substation with 20% of generation

The response on the system frequency with the shutdown of the generation at 20% of the PV station and HP is shown in Figure 4.16 The magnitude of the variation is high for same value of PV generation and that of Synchronous Generator. In comparison with the synchronous machine, the response of the PV is more oscillating, though is within the limits.

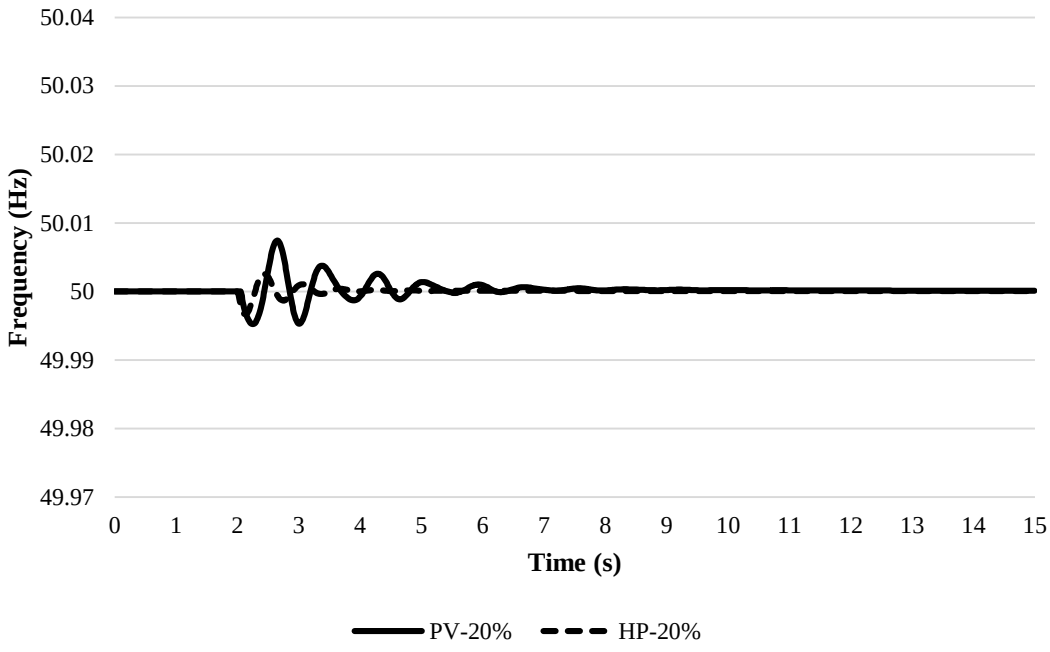

Figure 4.16: Frequency response on Devighat PH with 20% of generation

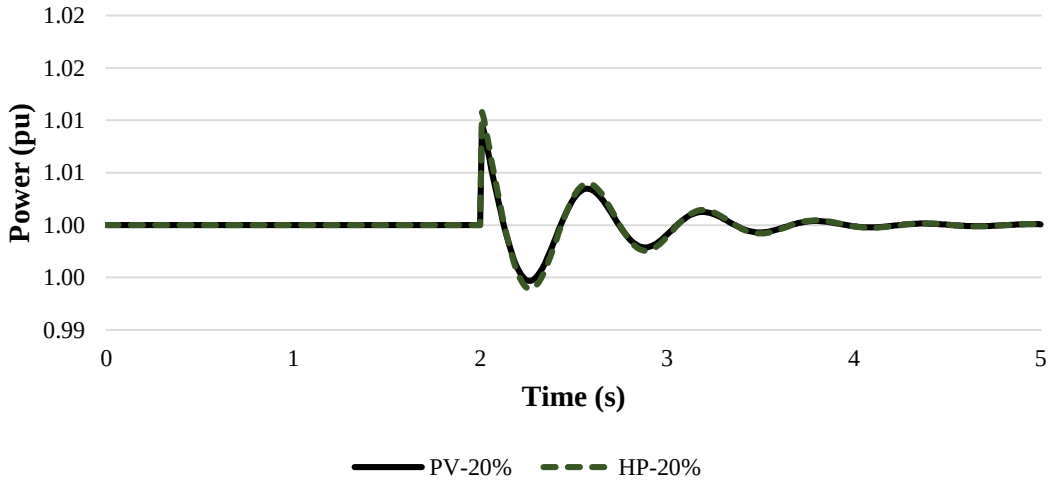

Figure 4.17: Power response on Devighat PH with 20% of generation

The Figure 4.17 infers that the oscillation in the power generation is for shorter duration than the frequency response. Also, the power generation of the nearby Devighat powerhouse fluctuates similarly for lower generation with the shutdown of the synchronous generator and the equivalent PV generation.

Case II: At 40% of the generation

In comparison with the equivalent size of the synchronous generator, the voltage drops more aggressively and also stabilizes quickly in case of the synchronous generator. So, the transient response is quicker in case of the synchronous machine with the equivalent size of hydro power as PV system as shown in Figure 4.18.

The Figure 4.19 shows the response on the frequency after the shutdown of the PV and generation system existing at 40% of the rated capacity after 2 seconds of operation. The response indicates that the oscillation in the generation caused due to the PV generation source is higher than the case of the synchronous generator. Moreover, the magnitude of the oscillation has increased for the higher value of generation as compared to the previous generation values.

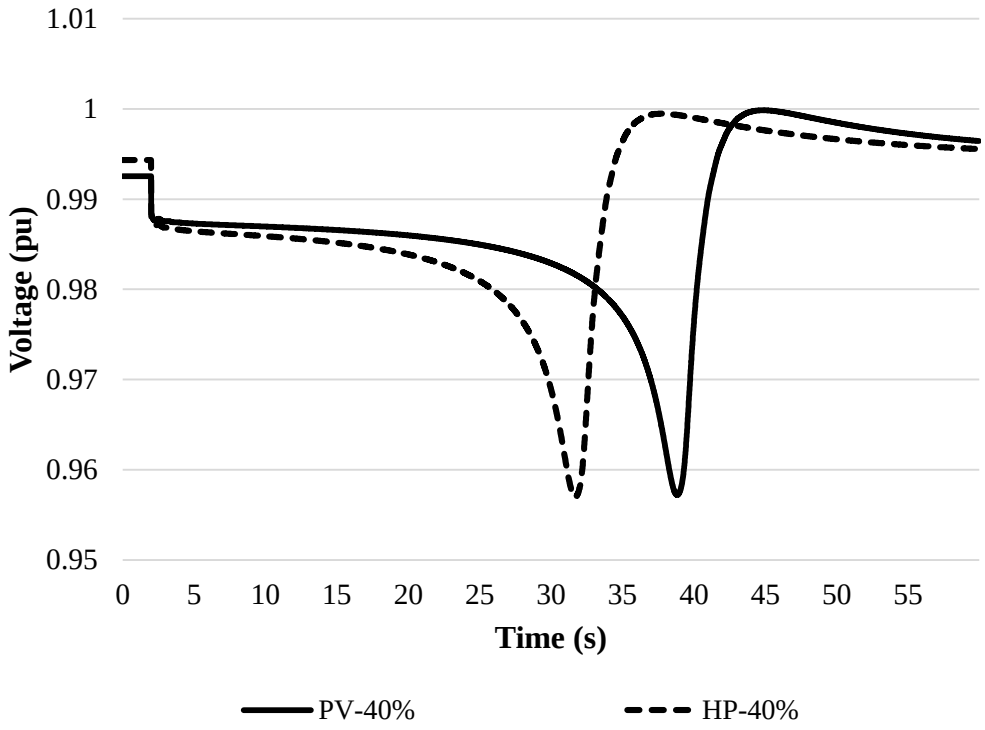

Figure 4.18: Voltage response on Devighat substation with 40% of generation

The Figure 4.20 shows the response on the power generation on the Devighat powerhouse with the shutdown of the generation of equivalent sizes connected to the Devighat powerhouse. The response shows that the fluctuation caused due to the synchronous generator is slightly higher than the inertia-less PV generation. However, the magnitude is within the acceptable range.

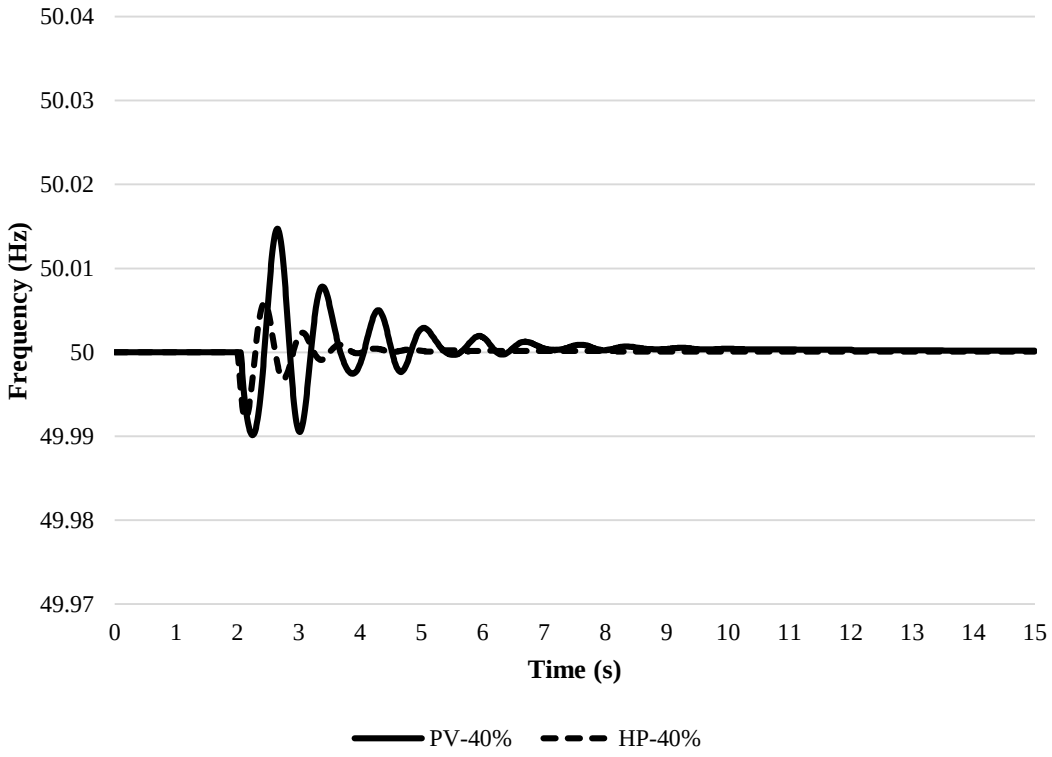

Figure 4.19: Frequency response on Devighat PH with 40% of generation

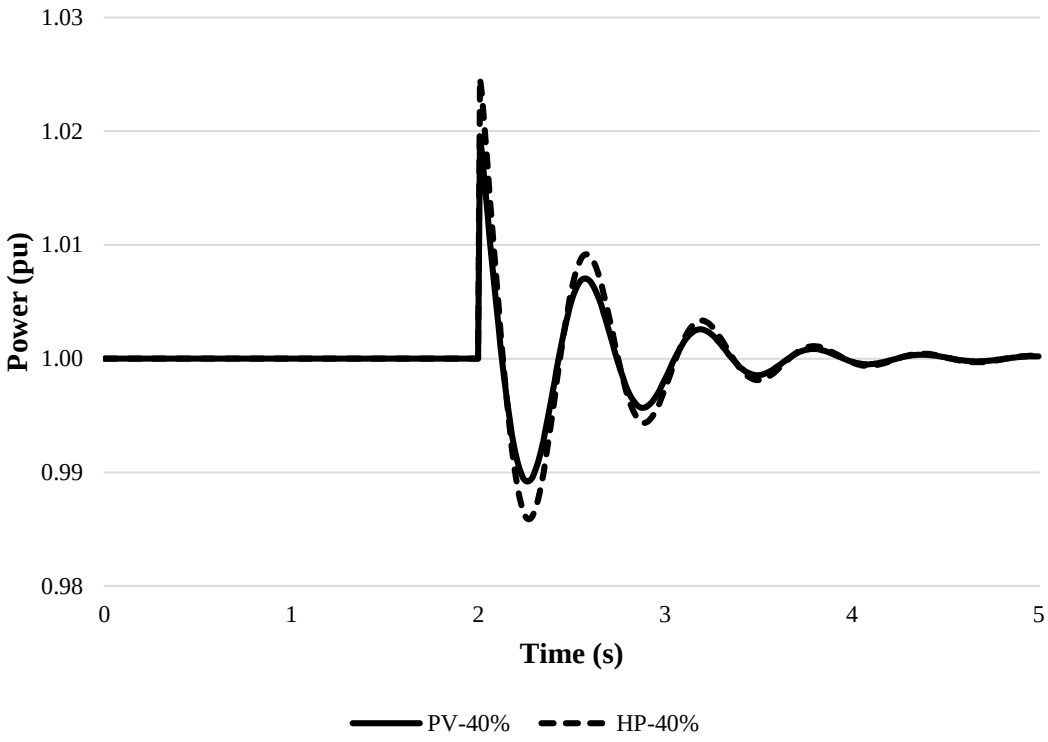

Figure 4.20:Power response on Devighat PH with 40% of generation

Case III: At 60% of the generation

In comparison with the generation at the lower capacity, the generation when made at the higher values, the response is observed for the quick interval i.e., reaches the minimum voltage quicker and also settles more quickly as shown in Figure 4.21. Similar, to the previous value of the generations, the response observed indicates that the drop in the voltage of the synchronous generator is higher than that of the PV generation.

With the shutdown of the same value of the generation initially at 60% capacity, the response on the system frequency is compared. The oscillation is much higher in the case of the PV generation than that of the equivalent synchronous machine as shown in Figure 4.22.

Moreover, the response on the power generation is slightly more fluctuating for the scenario of the synchronous machine than the same size of the photovoltaic system. The response on the first few seconds is steeply rising and for the next oscillations, the response is sinusoidal and decays after few oscillations. However, the oscillation is

within the range of 1.04pu and 0.98pu for both the systems and is within the limits as in Figure 4.23.

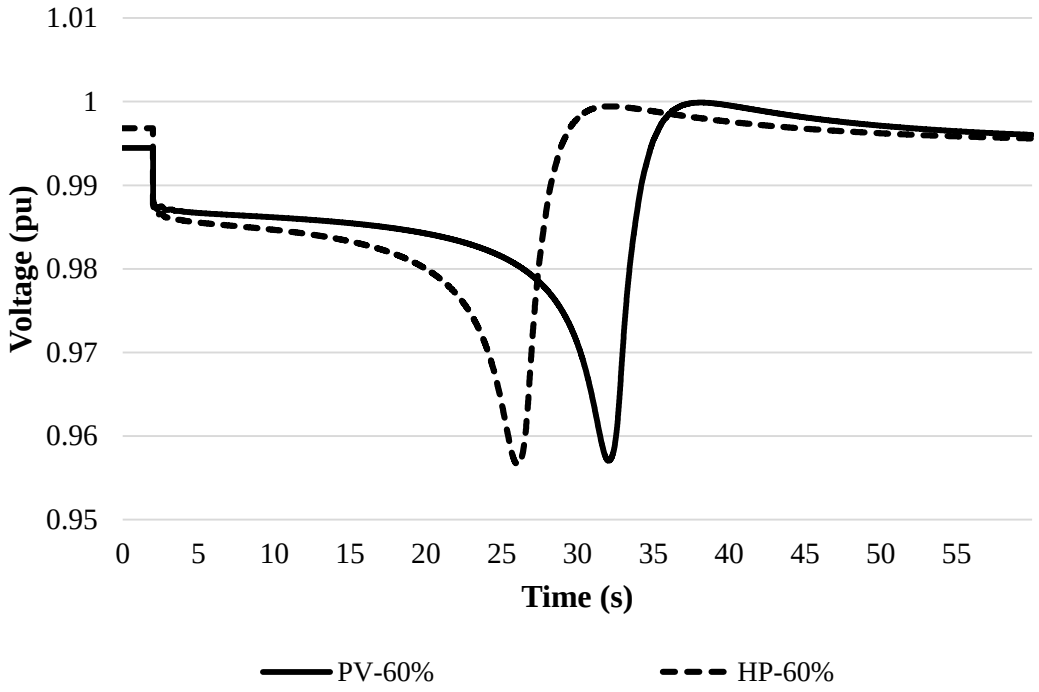

Figure 4.21: Voltage response on Devighat substation with 60% of generation

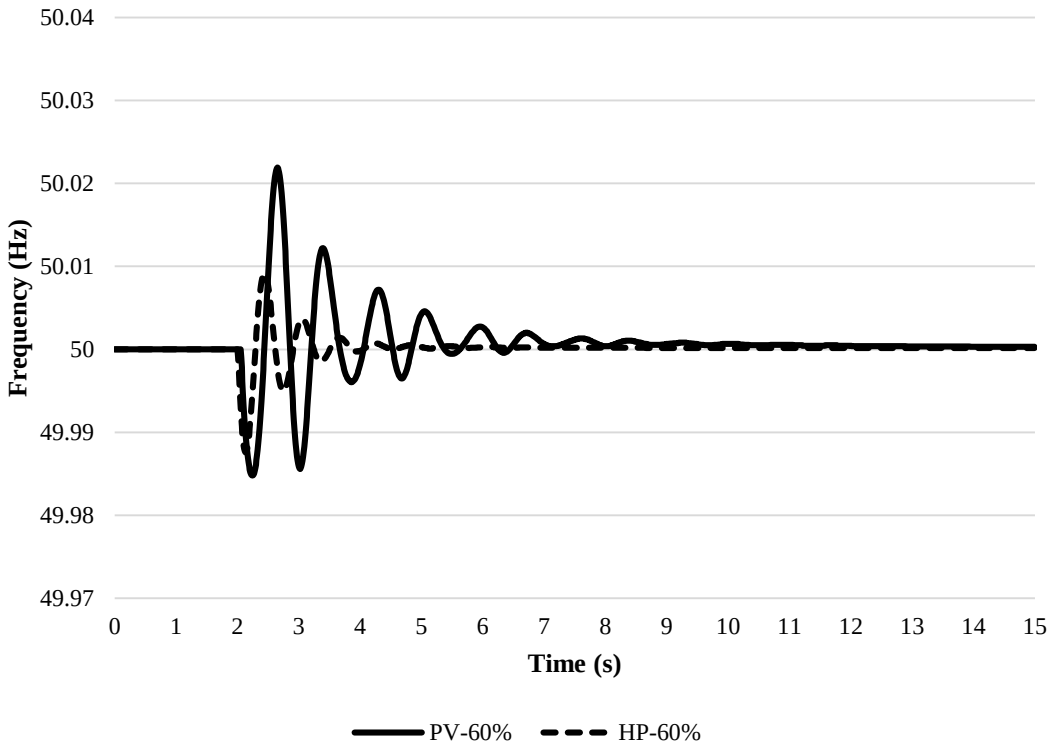

Figure 4.22: Frequency response on Devighat PH with 60% of generation

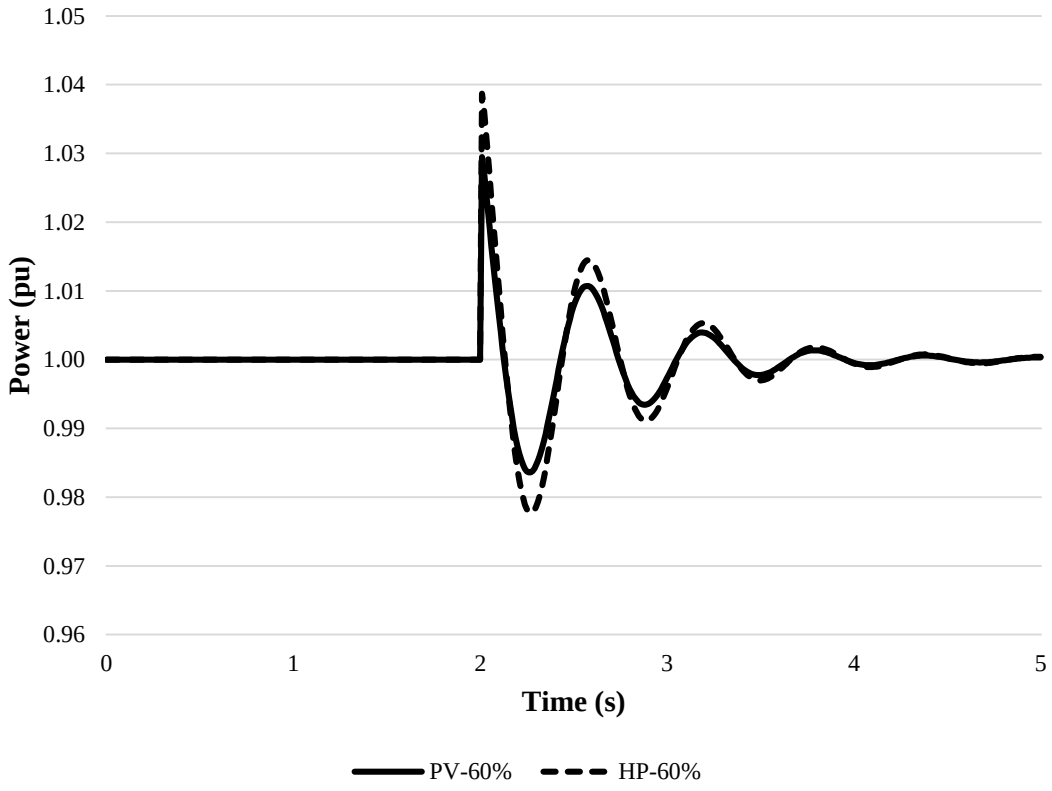

Figure 4.23: Power response on Devighat PH with 60% of generation

Case IV: At 80% of the generation

Similar, to the previous value of the generations, the response observed indicates that the drop in the voltage of the synchronous generator is higher than that of the PV generation. In comparison with the generation at the lower capacity, the generation when made at the higher values, the response is observed for the quick interval i.e., reaches the minimum voltage quicker and also settles more quickly as shown in Figure 4.24.

The oscillation is much higher for frequency response in the case of the PV generation than that of the equivalent synchronous machine as shown in Figure 4.25 but still is within the limits.

The oscillation in the power generation is within the range of 1.05pu and 0.97pu for both the systems and is within the limits as in Figure 4.26. The response on the power generation is slightly more fluctuating for the scenario of the synchronous machine than the same size of the photovoltaic system. As in the previous cases, the response on the first few seconds is steeply rising and for the next oscillations, the response is sinusoidal and decays after few oscillations.

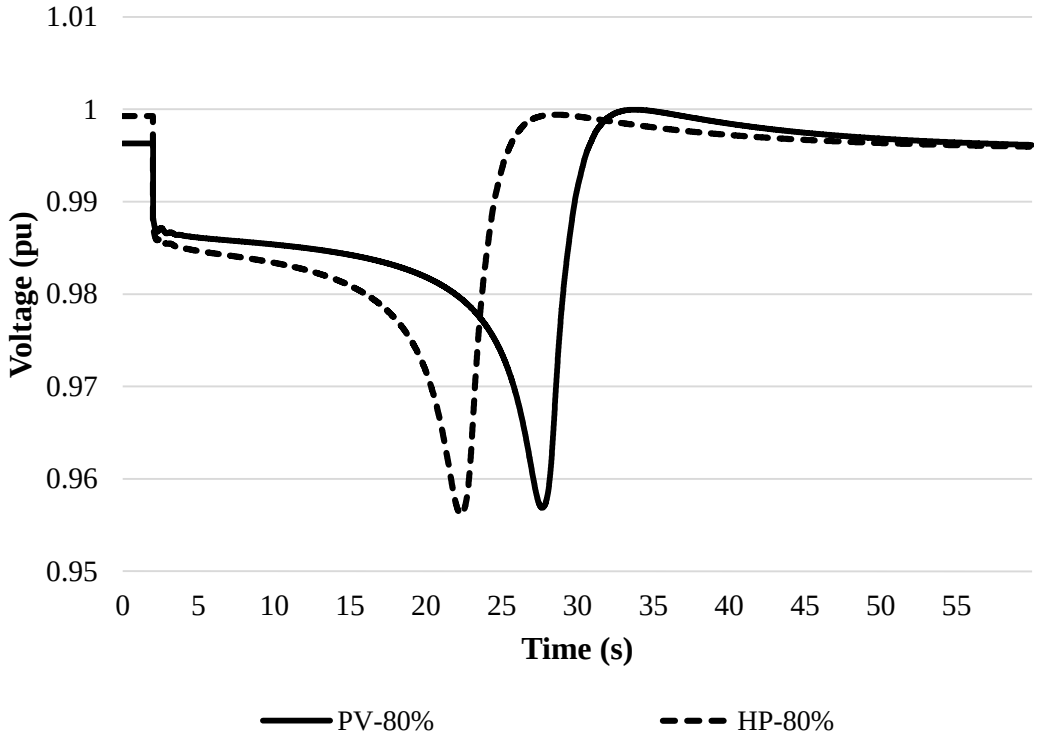

Figure 4.24: Voltage response on Devighat substation with 80% of generation

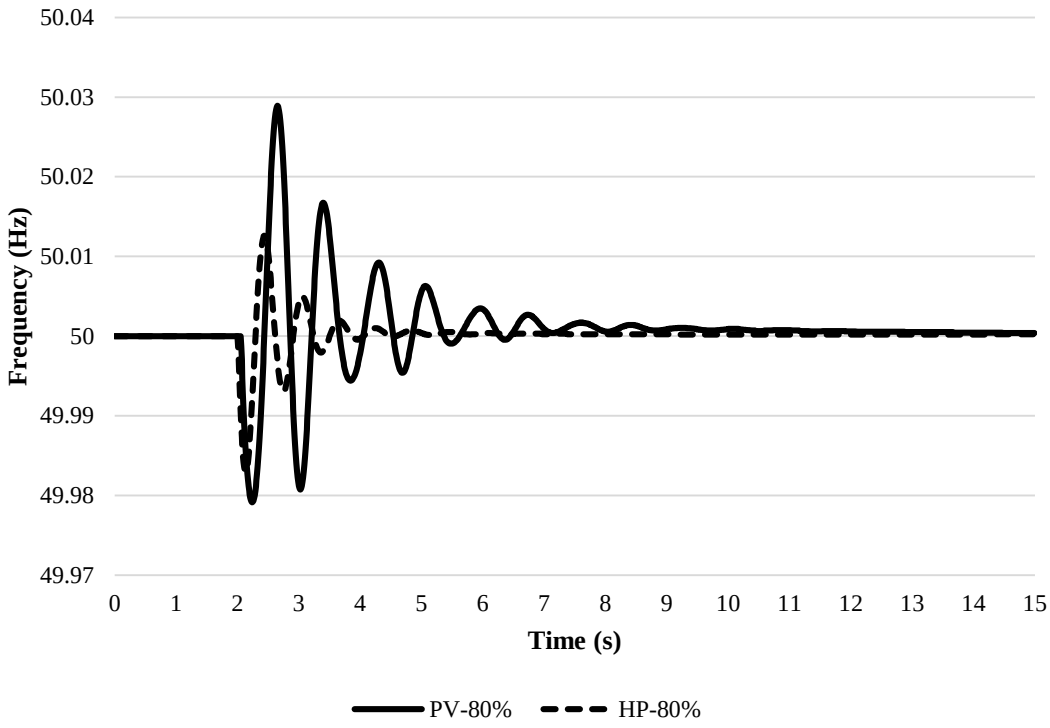

Figure 4.25: Frequency response on Devighat PH with 80% of generation

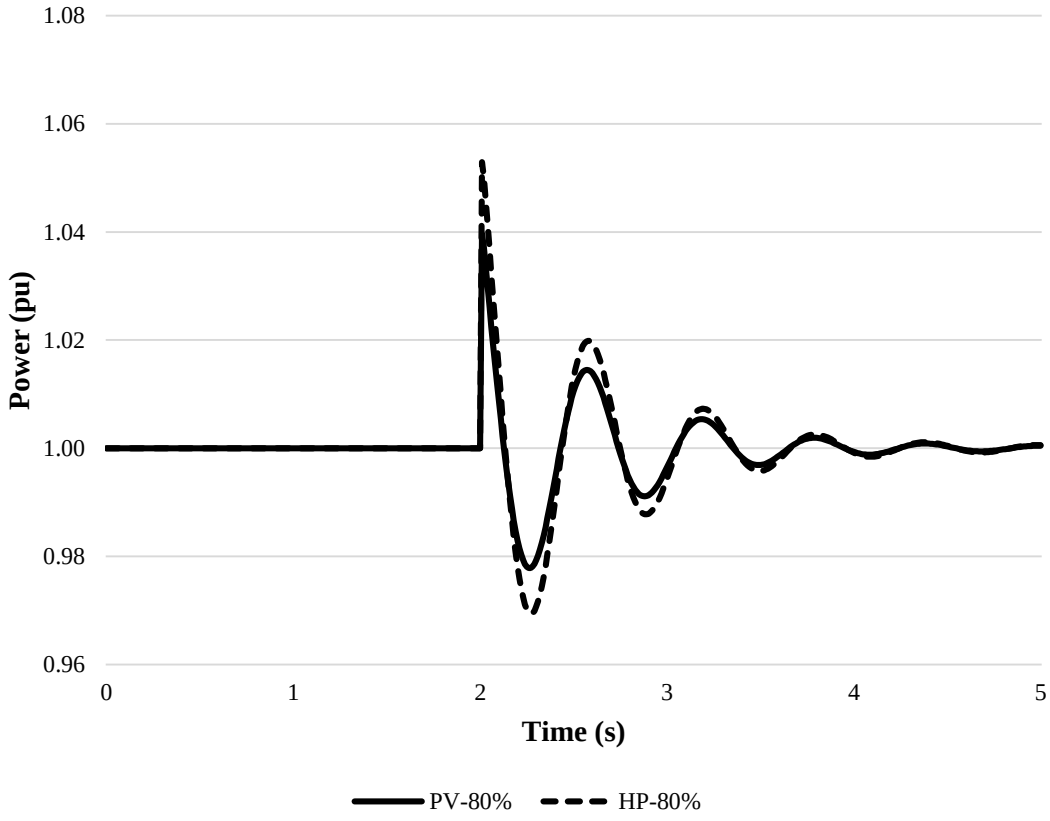

Figure 4.26: Power response on Devighat PH with 80% of generation

Case V: At 100% of the generation

Figure 4.27 shows that transient drop in the voltage is higher in case of the synchronous machine than the PV generation. Also, the response of the system is much quicker, the minimum transient voltage is reached faster and also, the transient value settles quicker for synchronous machine generation. The minimum voltage reached was about 0.956pu which is within the acceptable limits of the system. In comparison with the equivalent size of the PV, the voltage drops more aggressively and also stabilizes quickly in case of the synchronous generator. So, the transient response is quicker in case of the synchronous machine with the equivalent size of PV system.

The response on the system frequency with the shutdown of the same magnitudes of the PV station and synchronous machine is shown in Figure 4.28. The figure illustrates that the magnitude of variation is high for PV generation as compared with the synchronous machine, the response of the PV is more oscillating, though is within the limits.

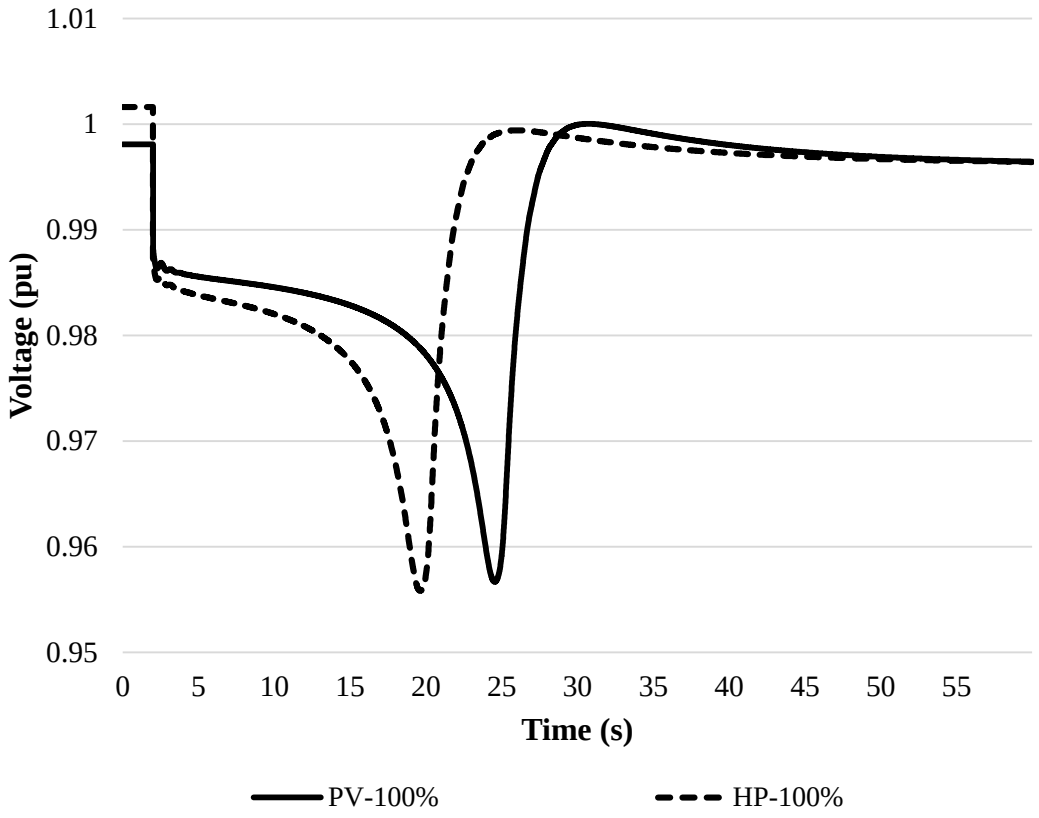

Figure 4.27:Voltage response on Devighat substation with 100% of generation

The Figure 4.29 infers that the oscillation in the power generation is for shorter duration than the frequency response. Also, the power generation of the nearby Devighat powerhouse fluctuates more with the shutdown of the synchronous generator than the equivalent PV generation.

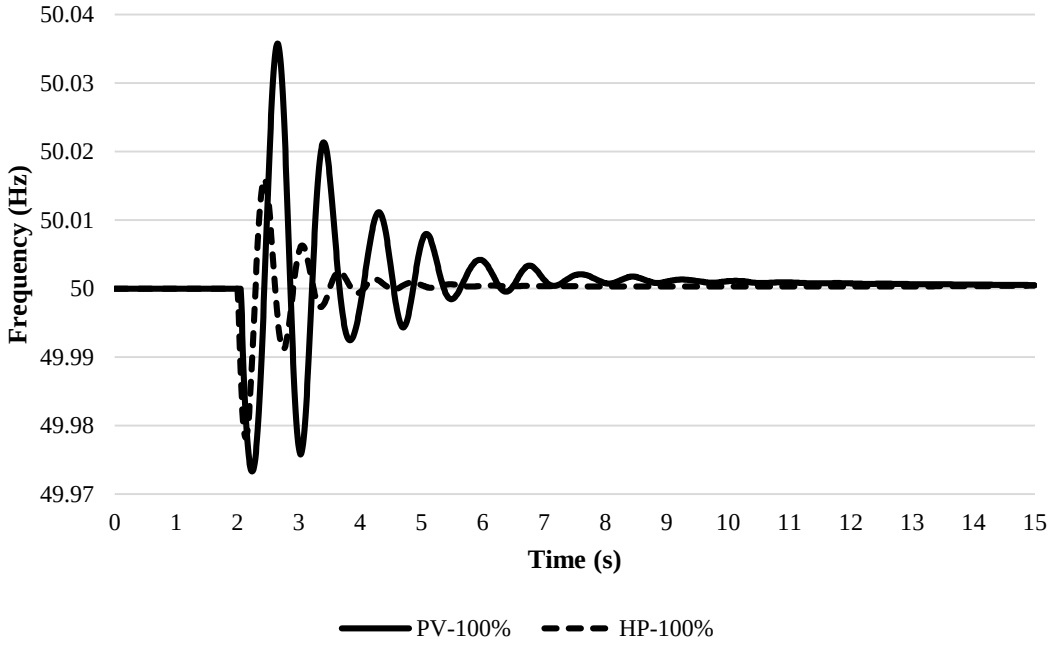

Figure 4.28: Frequency response on Devighat PH with 100% of generation

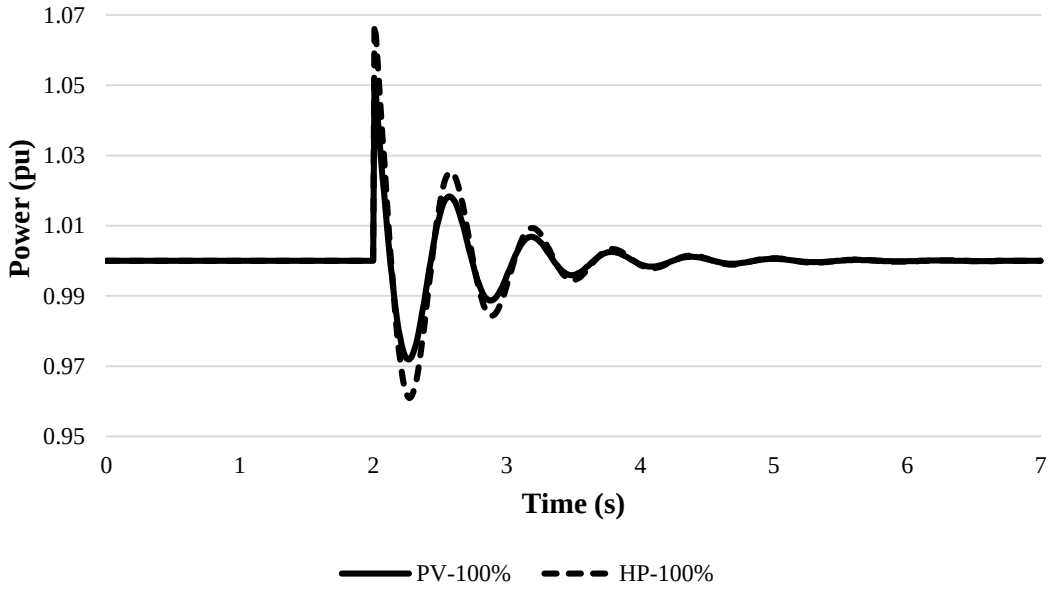

Figure 4.29: Power response on Devighat PH with 100% of generation

Case VI: For 46MW generation

The response on the system frequency with the shutdown of 46 MW of photovoltaic generation and generation from synchronous machine are shown in Figure 4.30. The figure illustrates that the magnitude of variation is high for PV generation as compared with the synchronous machine, but is within the standard limits.

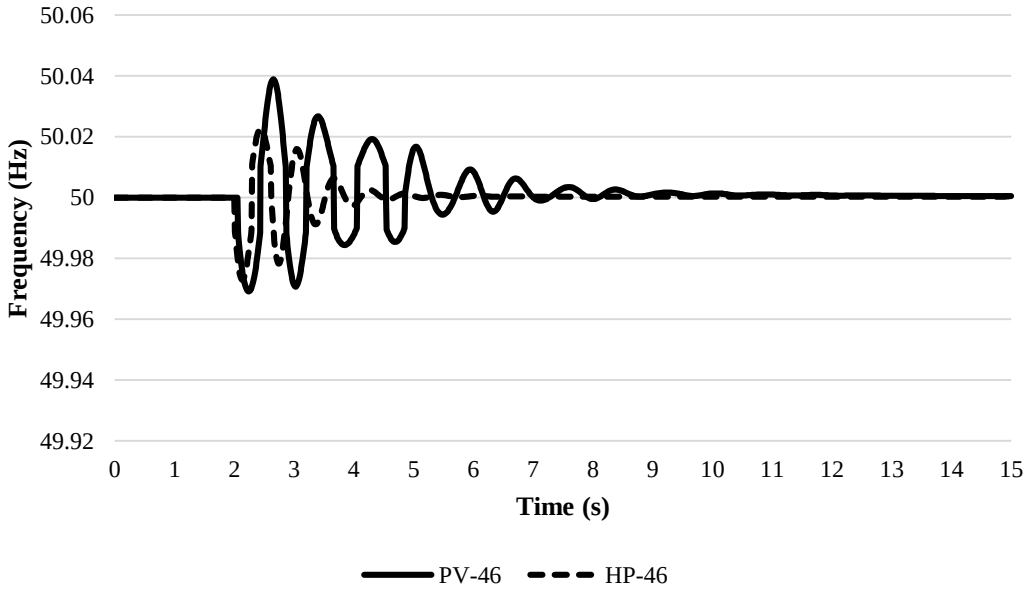

Figure 4.30: Frequency response on Devighat PH with 46MW of generation

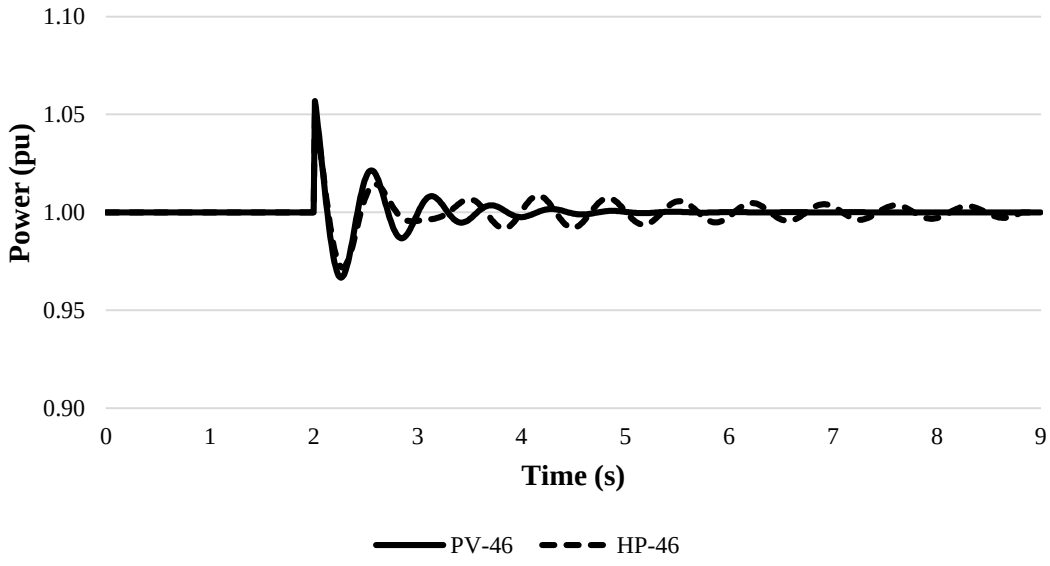

Figure 4.31: Power response on Devighat PH with 46MW of generation

The Figure 4.31 illustrates that the power generation of the nearby Devighat powerhouse fluctuates more with the shutdown of the synchronous generator than the equivalent PV generation.

Case VII: For 73MW generation

The transient response on system frequency with shutdown of 73MW of PV station and synchronous machine is shown in Figure 4.32. The figure illustrates that the magnitude of variation is high for PV generation as compared with the synchronous machine, the response of the PV is more oscillating, though is within the limits.

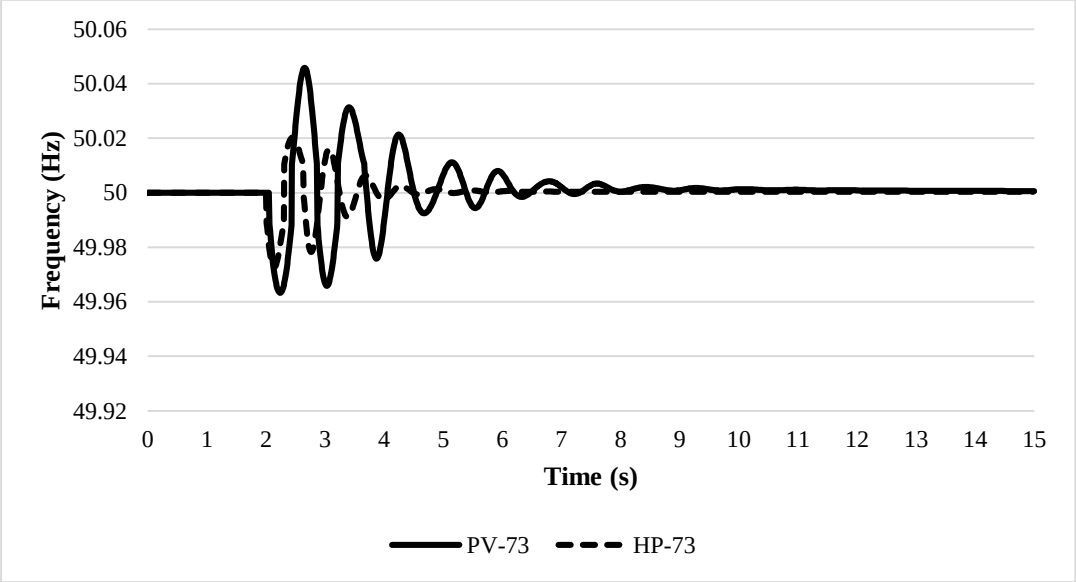

Figure 4.32: Frequency response on Devighat PH with 73MW of generation

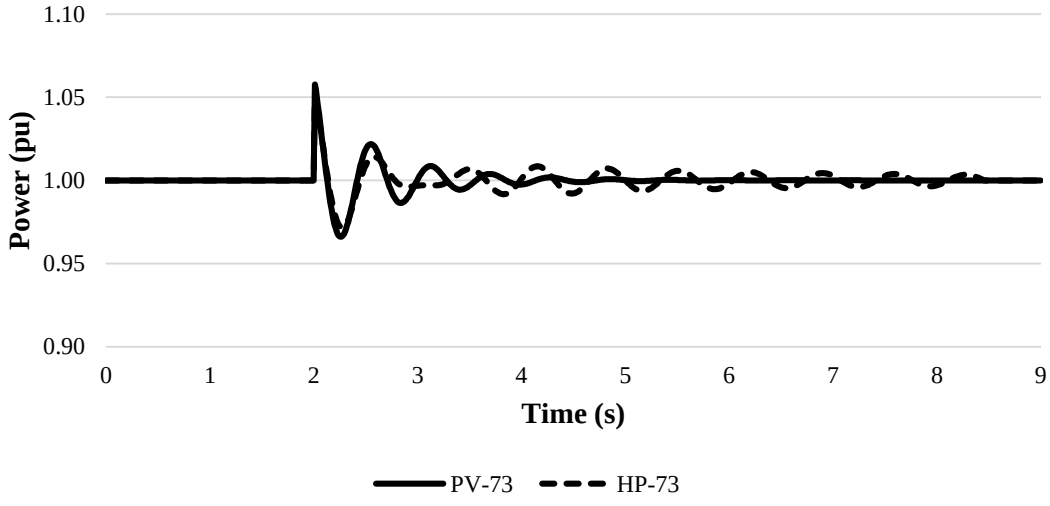

Figure 4.33: Power response on Devighat PH with 73MW of generation

The Figure 4.33 infers that the oscillation in the power generation is for shorter duration than the frequency response. Also, the power generation of the nearby Devighat powerhouse fluctuates more with the shutdown of the synchronous generator than the equivalent PV generation.

4.8 Small Signal Stability

The figure below shows the eigen plot of the system with the injection of a small amount of additional torque in the synchronous generator at Devighat power house. The additional torque equivalent to 0.1pu is added in the Devighat substation. This small additional torque can be due to the sudden decrease in the load. In this case, as shown in the Figure 4.34, all the eigen values are in the negative real parts representing that the system is stable under the small fluctuations in the initial parameters. It can also be seen as per the tabulation in Table 4.2. The eigen values are distributed over the negative axis, i.e. located at the open left half plane after the addition of PV to the system.

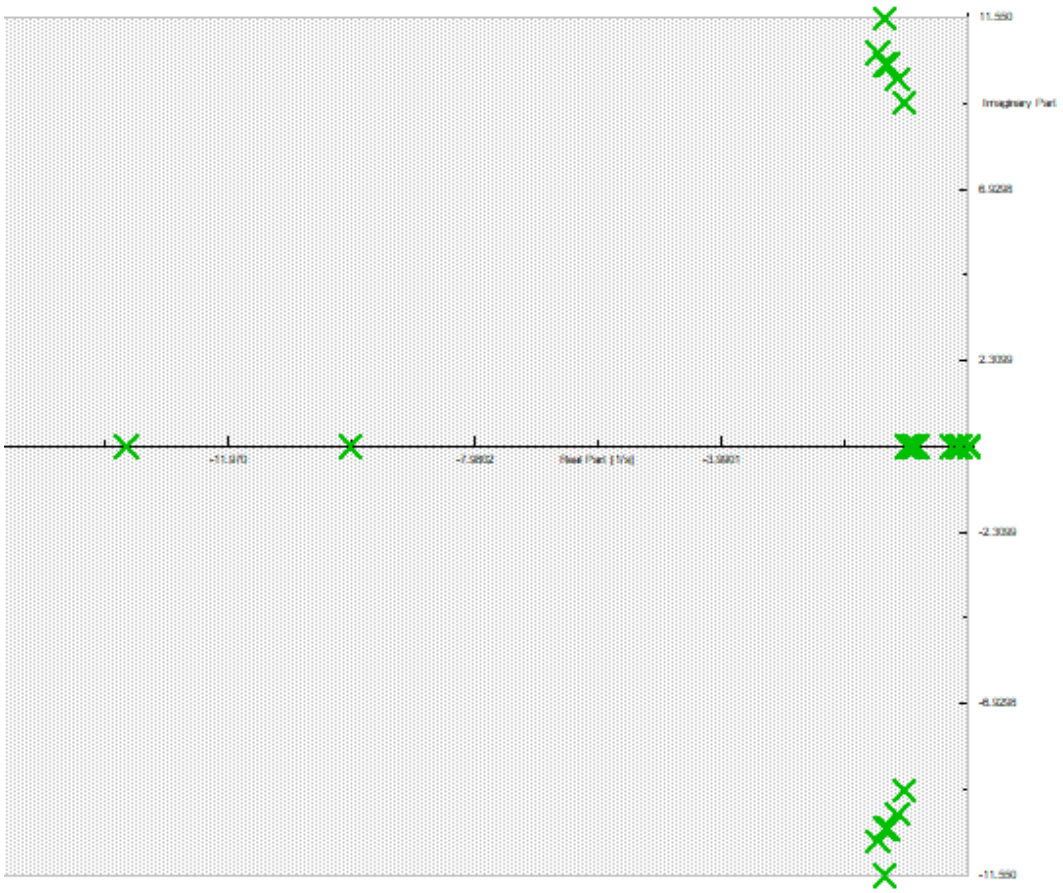

Figure 4.34: Small signal stability: eigen values for 25MW system.

Table 4.2: Eigen values for the 25MW Nuwakot PV system

Name	Real part	Imaginary part	Damped Frequency	Damping Ratio
	1/s	rad/s	Hz	
Mode 00001	-1	0	0	1
Mode 00002	-10	0	0	1
Mode 00003	-1	0	0	1
Mode 00004	-10	0	0	1
Mode 00005	0	0	0	0
Mode 00006	-1	0	0	1
Mode 00007	-10	0	0	1
Mode 00008	-1	0	0	1
Mode 00009	-10	0	0	1
Mode 00010	-1.359	11.54969	1.838190711	0.116859196
Mode 00011	-1.359	-11.5497	1.838190711	0.116859196
Mode 00012	-1.04335	9.257209	1.473330588	0.111997987
Mode 00013	-1.04335	-9.25721	1.473330588	0.111997987
Mode 00014	-1.46189	10.61824	1.689946122	0.136390311
Mode 00015	-1.46189	-10.6182	1.689946122	0.136390311
Mode 00016	-1.36366	10.29569	1.638610151	0.131303124
Mode 00017	-1.36366	-10.2957	1.638610151	0.131303124
Mode 00018	-1.30523	10.29255	1.638110656	0.125805123
Mode 00019	-1.30523	-10.2926	1.638110656	0.125805123
Mode 00020	-1.14939	9.907222	1.576783373	0.115242062
Mode 00021	-1.14939	-9.90722	1.576783373	0.115242062
Mode 00022	-19.9505	0	0	1
Mode 00023	-19.764	0	0	1
Mode 00024	-19.4666	0	0	1
Mode 00025	-19.1449	0	0	1
Mode 00026	-18.606	0	0	1
Mode 00027	-17.1005	0	0	1
Mode 00028	-17.4521	0.203256	0.03234916	0.999932186
Mode 00029	-17.4521	-0.20326	0.03234916	0.999932186
Mode 00030	-17.9381	0	0	1
Mode 00031	-17.5524	0	0	1
Mode 00032	-17.6876	0	0	1
Mode 00033	-17.816	0	0	1
Mode 00034	-0.83612	0	0	1
Mode 00035	-0.87261	0	0	1
Mode 00036	-0.9956	0	0	1
Mode 00037	-0.93416	0	0	1
Mode 00038	-0.95689	0	0	1
Mode 00039	-0.97949	0	0	1
Mode 00040	-0.28781	0	0	1

Name	Real part	Imaginary part	Damped Frequency	Damping Ratio
	1/s	rad/s	Hz	
Mode 00041	-0.11651	0	0	1
Mode 00042	-0.18129	0	0	1
Mode 00043	-0.16667	0	0	1
Mode 00044	-0.17516	0	0	1
Mode 00045	-0.14592	0	0	1
Mode 00046	-1.8E-07	0.015727	0.002503082	1.13916E-05
Mode 00047	-1.8E-07	-0.01573	0.002503082	1.13916E-05
Mode 00048	-1.6E-07	0	0	1
Mode 00049	0	0	0	0
Mode 00050	0	0	0	0

With the technical considerations, the PV is considered at 46MW and the eigen values for the system is performed and the results are presented in Figure 4.35. The figure shows all the eigenvalues with negative real part but two with purely imaginary parts, the real part of the eigen value has shifted the most and is the most critical one. Then the system shows oscillatory behavior in unstable conditions. The eigen values for the plot of the small signal effect in the system is illustrated in Table 4.3. From Table 4.3 it can be seen that for the Mode 00046 and Mode 00047, the real part of the eigen values is positive with negative damping constants representing the instability of the system.

Table 4.3: Eigen values for PV with 46MW in Devighat

Name	Real part	Imaginary part	Damped Frequency	Damping Ratio
	1/s	rad/s	Hz	
Mode 00001	-1	0	0	1
Mode 00002	-10	0	0	1
Mode 00003	-1	0	0	1
Mode 00004	-10	0	0	1
Mode 00005	0	0	0	0
Mode 00006	-1	0	0	1
Mode 00007	-10	0	0	1
Mode 00008	-1	0	0	1
Mode 00009	-10	0	0	1
Mode 00010	-1.359	11.5497	1.838192	0.11686
Mode 00011	-1.359	-11.5497	1.838192	0.11686
Mode 00012	-1.11233	9.082935	1.445594	0.121556
Mode 00013	-1.11233	-9.08294	1.445594	0.121556
Mode 00014	-1.4818	10.75724	1.712068	0.136461
Mode 00015	-1.4818	-10.7572	1.712068	0.136461
Mode 00016	-1.14944	9.906101	1.576605	0.115261

Name	Real part	Imaginary part	Damped Frequency	Damping Ratio
	1/s	rad/s	Hz	
Mode 00017	-1.14944	-9.9061	1.576605	0.115261
Mode 00018	-1.37362	10.31171	1.641159	0.132043
Mode 00019	-1.37362	-10.3117	1.641159	0.132043
Mode 00020	-1.30838	10.28883	1.637518	0.126149
Mode 00021	-1.30838	-10.2888	1.637518	0.126149
Mode 00022	-19.9504	0	0	1
Mode 00023	-19.764	0	0	1
Mode 00024	-19.4647	0	0	1
Mode 00025	-19.1448	0	0	1
Mode 00026	-18.606	0	0	1
Mode 00027	-17.099	0	0	1
Mode 00028	-17.8983	0	0	1
Mode 00029	-17.816	0	0	1
Mode 00030	-17.4159	0.087447	0.013918	0.999987
Mode 00031	-17.4159	-0.08745	0.013918	0.999987
Mode 00032	-17.6512	0	0	1
Mode 00033	-17.5445	0	0	1
Mode 00034	-0.8343	0	0	1
Mode 00035	-0.87259	0	0	1
Mode 00036	-0.9956	0	0	1
Mode 00037	-0.93415	0	0	1
Mode 00038	-0.9566	0	0	1
Mode 00039	-0.97949	0	0	1
Mode 00040	-0.28781	0	0	1
Mode 00041	-0.16598	0	0	1
Mode 00042	-0.18042	0	0	1
Mode 00043	-0.17515	0	0	1
Mode 00044	-0.14592	0	0	1
Mode 00045	-0.0467	0	0	1
Mode 00046	3.75E-07	0.015721	0.002502	-2.4E-05
Mode 00047	3.75E-07	-0.01572	0.002502	-2.4E-05
Mode 00048	-1.6E-07	0	0	1
Mode 00049	0	0	0	0
Mode 00050	0	0	0	0

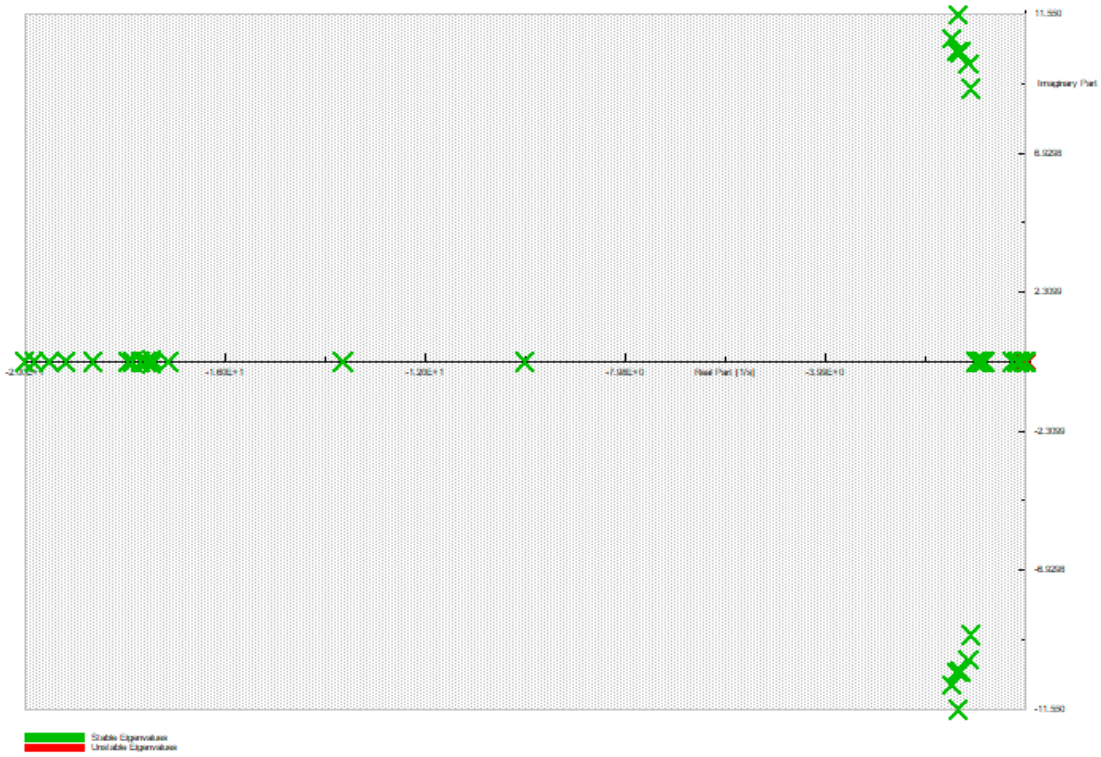

Figure 4.35: Small signal stability: eigen values for 46MW PV system

Table 4.4: Participation factors for the critical modes with 46MW PV generation

Object	State Variable	Participation: Mag.	Participation: Angle
Bhotekoshi HP	phi	4.6765E-08	-112.3168433
Bhotekoshi HP	psiD	2.00826E-06	-89.60053236
Bhotekoshi HP	psiQ	2.06E-09	-89.60610108
Bhotekoshi HP	psie	3.16705E-05	-89.60053236
Bhotekoshi HP	psix	3.2482E-08	-89.60610111
Bhotekoshi HP	speed	5.43E-10	64.52718434
Chilime PH	phi	8.5606E-08	163.9434409
Chilime PH	psiD	9.67664E-06	89.97852688
Chilime PH	psiQ	1.9351E-08	90.03120415
Chilime PH	psie	0.000152601	89.97852688
Chilime PH	psix	3.05164E-07	90.03120414
Chilime PH	speed	2.9239E-08	97.80293763
Devighat PH	phi	1.4484E-08	162.1349569
Devighat PH	psiD	4.64062E-07	90.89406798
Devighat PH	psiQ	4.7E-10	91.04999105
Devighat PH	psie	7.31831E-06	90.89406798
Devighat PH	psix	7.407E-09	91.04999108
Devighat PH	speed	2.6535E-08	176.8361757
Khimti HP	phi	3.07933E-07	-31.63405953
Khimti HP	psiD	7.75782E-07	-89.83538856

Object	State Variable	Participation: Mag.	Participation: Angle
Khimti HP	psiQ	2.9E-10	-89.94804737
Khimti HP	psie	1.22342E-05	-89.83538856
Khimti HP	psix	4.571E-09	-89.94804745
Khimti HP	speed	1.16625E-07	179.8525539
Trishuli PH	phi	2.3182E-08	162.2740427
Trishuli PH	psiD	8.06129E-07	90.99112923
Trishuli PH	psiQ	8.76E-10	91.13677415
Trishuli PH	psie	1.27127E-05	90.99112923
Trishuli PH	psix	1.3807E-08	91.13677426
Trishuli PH	speed	3.8959E-08	176.1303226
Upper Tamakoshi	phi	2.77839E-06	-14.80299041
Upper Tamakoshi	psiD	3.66557E-07	88.9051817
Upper Tamakoshi	psiQ	5.59E-10	91.71514139
Upper Tamakoshi	psie	5.78063E-06	88.9051817
Upper Tamakoshi	psix	8.823E-09	91.71514143
Upper Tamakoshi	speed	1.36551E-06	179.7177498

For the same size of synchronous machine considered, the eigen values are so obtained that all those lies in the negative axis indicating the stable operation as shown in Figure 4.36 and Table 4.5.

Table 4.5: Eigen values for the 46MW synchronous machine

Name	Real part	Imaginary part	Damped Frequency	Damping Ratio
	1/s	rad/s	Hz	
Mode 00001	-1	0	0	1
Mode 00002	-10	0	0	1
Mode 00003	-1	0	0	1
Mode 00004	-10	0	0	1
Mode 00005	-1	0	0	1
Mode 00006	-10	0	0	1
Mode 00007	0	0	0	0
Mode 00008	-1	0	0	1
Mode 00009	-10	0	0	1
Mode 00010	-49.89187061	0	0	1
Mode 00011	-22.05158979	31.31470446	4.983890006	0.575760834
Mode 00012	-22.05158979	-31.31470446	4.983890006	0.575760834
Mode 00013	-1.358995889	11.54972249	1.838195426	0.116858635
Mode 00014	-1.358995889	-11.54972249	1.838195426	0.116858635
Mode 00015	-0.934105793	8.837221485	1.406487483	0.105115714
Mode 00016	-0.934105793	-8.837221485	1.406487483	0.105115714
Mode 00017	-1.463230459	10.64883303	1.694814415	0.136128487

Name	Real part	Imaginary part	Damped Frequency	Damping Ratio
	1/s	rad/s	Hz	
Mode 00018	-1.463230459	-10.64883303	1.694814415	0.136128487
Mode 00019	-1.381665395	10.38806733	1.653312265	0.131843978
Mode 00020	-1.381665395	-10.38806733	1.653312265	0.131843978
Mode 00021	-1.298900507	10.29515122	1.638524206	0.125173918
Mode 00022	-1.298900507	-10.29515122	1.638524206	0.125173918
Mode 00023	-1.199192143	9.840196324	1.566115886	0.120971695
Mode 00024	-1.199192143	-9.840196324	1.566115886	0.120971695
Mode 00025	-1.149181085	9.907670503	1.576854735	0.115216588
Mode 00026	-1.149181085	-9.907670503	1.576854735	0.115216588
Mode 00027	-19.95262539	0	0	1
Mode 00028	-19.63458134	0	0	1
Mode 00029	-19.76398537	0	0	1
Mode 00030	-19.14856658	0	0	1
Mode 00031	-18.79294601	0	0	1
Mode 00032	-18.60586204	0	0	1
Mode 00033	-16.76905701	0	0	1
Mode 00034	-17.10490308	0	0	1
Mode 00035	-17.38491585	0.294721055	0.046906313	0.999856334
Mode 00036	-17.38491585	-0.294721055	0.046906313	0.999856334
Mode 00037	-17.93441839	0	0	1
Mode 00038	-17.56311877	0	0	1
Mode 00039	-17.77194488	0	0	1
Mode 00040	-17.81603455	0	0	1
Mode 00041	-0.343869071	0.364539205	0.058018216	0.686182586
Mode 00042	-0.343869071	-0.364539205	0.058018216	0.686182586
Mode 00043	-0.811562652	0	0	1
Mode 00044	-0.872559956	0	0	1
Mode 00045	-0.995855699	0	0	1
Mode 00046	-0.927535674	0	0	1
Mode 00047	-0.935149714	0	0	1
Mode 00048	-0.974664821	0	0	1
Mode 00049	-0.979492696	0	0	1
Mode 00050	-0.287811803	0	0	1
Mode 00051	-5.68743E-07	0.015718319	0.002501648	3.61834E-05
Mode 00052	-5.68743E-07	-0.015718319	0.002501648	3.61834E-05
Mode 00053	-0.109511984	0	0	1
Mode 00054	-0.168418872	0	0	1
Mode 00055	-0.18184896	0	0	1
Mode 00056	-0.175165574	0	0	1
Mode 00057	-0.145922546	0	0	1
Mode 00058	-1.35811E-07	0	0	1

Name	Real part	Imaginary part	Damped Frequency	Damping Ratio
	1/s	rad/s	Hz	
Mode 00059	-5	5	0.795774715	0.707106781
Mode 00060	-5	-5	0.795774715	0.707106781
Mode 00061	0	0	0	0
Mode 00062	0	0	0	0
Mode 00063	-10	0	0	1
Mode 00064	-5	0	0	1
Mode 00065	0	0	0	0

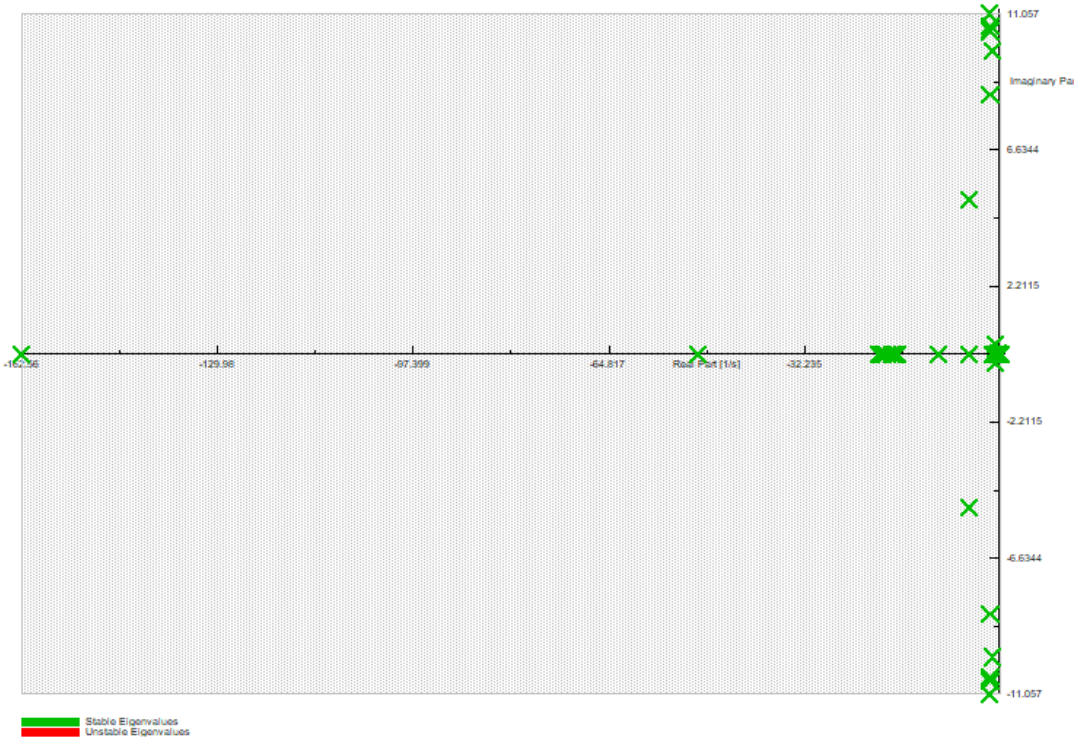

Figure 4.36: Small signal stability: eigen values for 46MW synchronous system

CHAPTER FIVE: CONCLUSION AND RECOMMENDATIONS

The various conclusions and recommendations have been obtained from study.

5.1 Conclusion

From the above analysis, the following conclusions can be drawn:

- The annual performance of the solar plant is about 0.8 times the rated capacity.
- With the placement of PV at location distant from the load center, the overall loss can increase with significant improvement of the voltages at nearby bus and the rest remains unaffected. The loss has increased for the Kathmandu valley from the existing value of 3.47% to 3.96%.
- The fluctuation in system frequency is higher for the PV than the synchronous generator. Moreover, the response in the active power generation and voltage in the nearby source is slightly higher for synchronous machine. The deviation is higher for the large level of the generation.
- The small signal stability eigen values indicate that the system is in stable state with small change in the initial parameters. The PV generation is increased to the technically viable limit and it was observed that the system may be unstable with the damping constant for Mode 00046 and Mode 00047 obtained negative. While for the same size of synchronous generation is stable. So, the system stability might be compromised with the addition of higher value of inertia-less PV generation source.

5.2 Recommendations

Following recommendations have been made from the study:

- The future extension of this study can be performed for the other PV stations under construction and proposed over the country.
- The generalizations can be done for the effect of wind and PV systems integrated in the overall INPS grid network.

REFERENCES

Abdalla, O. H., Al-Badwawi, R., Al-Hadi, H., Al-Riyami, H., & Al-Nadabi, A. (2012). Impact of a 200 MW concentrated receiver solar power plant on steady-state and transient performances of Oman transmission system. *2012 IEEE International Power Engineering and Optimization Conference, PEOCO 2012 - Conference Proceedings*, *June 2012*, 401–406. https://doi.org/10.1109/PEOCO.2012.6230897

Al-Akayshee, A. S., Kuznetsov, O. N., Alwazah, I., & Deeb, M. (2020). Investigation of the Performance of Iraqi 400kV Electrical Network in DIgSILENT Power Factory. In IEEE (Ed.), *Proceedings of the 2nd 2020 International Youth Conference on Radio Electronics, Electrical and Power Engineering, REEPE 2020*. 2020 International Youth Conference on Radio Electronics, Electrical and Power Engineering (REEPE). https://doi.org/10.1109/REEPE49198.2020.9059208

Bogdanov, D., Gulagi, A., Fasihi, M., & Breyer, C. (2021). Full energy sector transition towards 100% renewable energy supply: Integrating power, heat, transport and industry sectors including desalination. *Applied Energy*, *283*(xxxx), 116273. https://doi.org/10.1016/j.apenergy.2020.116273

Borsche, T. S., Ulbig, A., & Andersson, G. (2014). Impact of frequency control reserve provision by storage systems on power system operation. *IFAC Proceedings Volumes (IFAC-PapersOnline)*, *19*, 4038–4043. https://doi.org/10.3182/20140824-6-za-1003.02257

Denholm, P., Mai, T., Kenyon, R. W., Kroposki, B., & Malley, M. O. (2020). Inertia and the Power Grid : A Guide Without the Spin. *National Renewable Energy Laboratory*, *May*, 48. https://www.nrel.gov/docs/fy20osti/73856.pdf

Global Solar Atlas. (2022). https://globalsolaratlas.info

Gogoi, K., Mishra, D., Debnath, N., Chatterjee, S., & Datta, B. (2016). Modelling and study of steady state analysis and fault parameters in 400 kV and 220kV buses of Indian North Eastern Regional Grid. *2015 International Conference on Energy, Power and Environment: Towards Sustainable Growth, ICEPE 2015*, 0–4.

https://doi.org/10.1109/EPETSG.2015.7510139

Gulagi, A., Pathak, S., Bogdanov, D., & Breyer, C. (2021). Renewable Energy Transition for the Himalayan Countries Nepal and Bhutan: Pathways towards Reliable, Affordable and Sustainable Energy for All. *IEEE Access*, *9*, 84520–84544. https://doi.org/10.1109/ACCESS.2021.3087204

IFC. (2015). *Utility-Scale Solar Photovoltaic Power Plants*. 35–39.

Johnson, S. C., Papageorgiou, D. J., Mallapragada, D. S., Deetjen, T. A., Rhodes, J. D., & Webber, M. E. (2019). Evaluating rotational inertia as a component of grid reliability with high penetrations of variable renewable energy. *Energy*, *180*, 258–271. https://doi.org/10.1016/j.energy.2019.04.216

Khadka, N., Bista, A., Adhikari, B., Shrestha, A., Bista, D., & Adhikary, B. (2020). Current Practices of Solar Photovoltaic Panel Cleaning System and Future Prospects of Machine Learning Implementation. *IEEE Access*, *8*, 135948–135962. https://doi.org/10.1109/ACCESS.2020.3011553

Nikolaev, N., Dimitrov, K., & Rangelov, Y. (2021). A comprehensive review of small-signal stability and power oscillation damping through photovoltaic inverters. *Energies*, *14*(21). https://doi.org/10.3390/en14217372

Ogino, K., Dash, S. K., & Nakayama, M. (2019). Change to hydropower development in Bhutan and Nepal. *Energy for Sustainable Development*, *50*, 1–17. https://doi.org/10.1016/j.esd.2019.02.005

Panjwani, M. K., & Narejo, G. B. (2014). *Effect of Altitude on the Efficiency of Solar Panel*. *2*(4), 461–464. http://ijergs.org/files/documents/EFFECT-57.pdf

Parmar, D., & Mehta, D. B. (2018). *Small Signal Stability Analysis of Power System with Increased Penetration of PV Generation*. *1*, 200–191. https://doi.org/10.29007/zktd

Quan, H., Li, B., Xiu, X., & Hui, D. (2017). Impact analysis for high-penetration distributed photovoltaic generation integrated into grid based on DIgSILENT. *2017 IEEE Conference on Energy Internet and Energy System Integration, EI2 2017 - Proceedings*, *2018-Janua*, 1–6. https://doi.org/10.1109/EI2.2017.8245606

Remon, D., Cantarellas, A. M., Mauricio, J. M., & Rodriguez, P. (2017). Power system

stability analysis under increasing penetration of photovoltaic power plants with synchronous power controllers. *IET Renewable Power Generation*, *11*(6), 733–741. https://doi.org/10.1049/iet-rpg.2016.0904

Sadhana, S. G., Ashok, S., & Kumaravel, S. (2017). Small Signal Stability Analysis of Grid Connected Renewable Energy Resources with the Effect of Uncertain Wind Power Penetration. *Energy Procedia*, *117*, 769–776. https://doi.org/10.1016/j.egypro.2017.05.193

Shinn, L. (2018). *Renewable Energy: The Clean Facts*. https://www.nrdc.org/stories/renewable-energy-clean-facts

Srivastava, A., Meena, R., & Parida, S. K. (2018). Effect of PV and FACTS on Small Signal Stability. *2018 20th National Power Systems Conference, NPSC 2018*. https://doi.org/10.1109/NPSC.2018.8771832

Toma, R., & Gavrilas, M. (2016). Voltage stability assessment for wind farms integration in electricity grids with and without consideration of voltage dependent loads. *Proceedings of the 2016 International Conference and Exposition on Electrical and Power Engineering, EPE 2016*, *Epe*, 754–759. https://doi.org/10.1109/ICEPE.2016.7781440

Ulbig, A., Borsche, T. S., & Andersson, G. (2014). Impact of low rotational inertia on power system stability and operation. *IFAC Proceedings Volumes (IFAC-PapersOnline)*, *19*, 7290–7297. https://doi.org/10.3182/20140824-6-za-1003.02615

Ulbig, A., Borsche, T. S., & Andersson, G. (2015). Analyzing Rotational Inertia, Grid Topology and their Role for Power System Stability. *IFAC-PapersOnLine*, *48*(30), 541–547. https://doi.org/10.1016/j.ifacol.2015.12.436

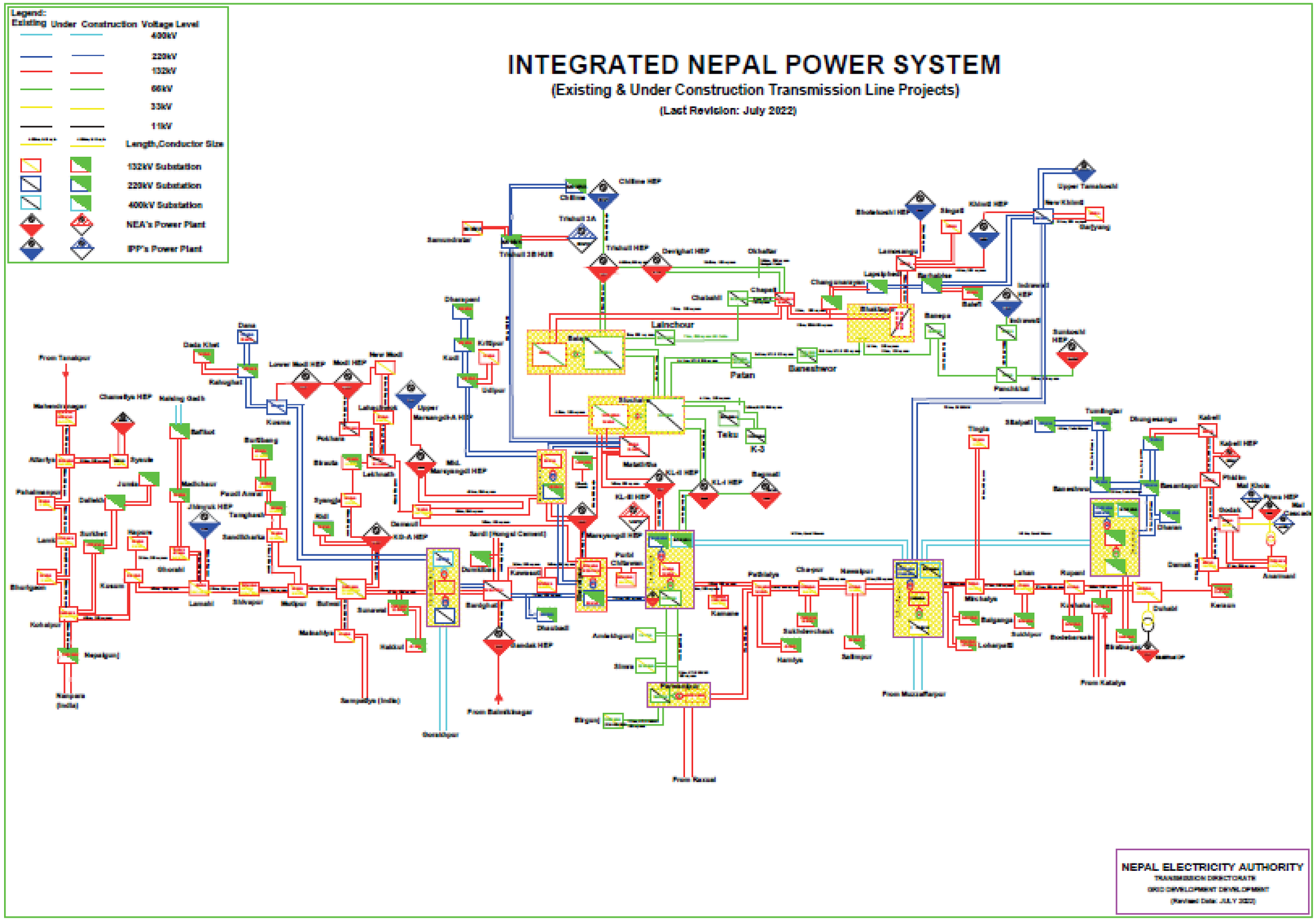

Figure A.1: INPS of Nepal (Source: NEA)

Table A.1: Load demand of the grid substations

S.N.	Substation Name	MVA	MW	MVAR
1	Balaju	29.72	26.75	12.95
2	Baneshwor	27.55	24.8	12.01
3	Bhaktapur	31.79	28.61	13.86
4	Chapali	33.91	30.52	14.78
5	K3	29.32	26.39	12.78
6	Lainchour	32	27.2	16.86
7	Lamosanghu	17.49	15.74	7.62
8	New Chabahil	33.91	30.52	14.78
9	Patan	41.9	37.71	18.26
10	Suichatar	20.52	18.46	8.94
11	Teku	23.9	21.51	10.42

Table A.2: Line Parameters of the interconnected INPS Data

S.N.	From	To	Line Impedance		
			Positive		
			R	X	Y
1	Bhotekoshi PH	Lamosanghu	3.38	12.09	81.07
2	Trishuli HP	Balaju	3.97	5.86	161.53
3	Chilime	Trishuli HP	7.14	15.87	101.99
4	Devighat PH	Trishuli HP	0.83	1.86	11.92
5	Okhaltar	Devighat PH	3.63	5.36	147.61
6	Okhaltar	Chapali	0.08	0.49	15.60
7	Suichatar	Teku	0.23	0.75	22.84
8	Khimti	Lamosanghu	1.38	2.88	92.34
9	K3	Teku	0.08	0.49	15.60
10	Suichatar	Patan	0.59	1.25	36.21
11	Baneshwor	Patan	0.71	1.13	7.06
12	Balaju	Suichatar	0.64	1.35	38.99
13	Balaju	Lainchour	0.27	0.80	5.23
14	New Chabel	Lainchour	0.39	2.59	18.31
15	Chapali	New Chabahil	0.69	1.01	27.85
16	Chapali	Bhaktapur	0.66	2.21	66.84
17	Bhaktapur	Baneshwor	3.42	5.43	34.00

Table A.3: Generation capacities of Power houses near Kathmandu Valley

S.N.	Name	Generation capacity (MW)
1	Trishuli	21
2	Devighat	14.1
3	Chilime	22
4	Bhotekoshi	36
5	Khimti	60
6	Marsyangdi	50+69+69
7	Kulekhani	32
8	Tamakoshi	456

Meteo for Devighat - Synthetically generated data from monthly values.

Interval beginning	GlobHor kWh/m²/mth	DiffHor kWh/m²/mth
January	117.7	38.2
February	110.5	52.3
March	167.5	64.0
April	176.1	79.4
May	193.2	91.3
June	174.9	95.3
July	156.8	86.2
August	164.2	80.9
September	145.9	68.7
October	158.2	50.5
November	133.5	30.2
December	126.4	27.9
Year	1824.8	765.0

Figure A.2: Irradiance data obtained from Meteonorm 8.0 for Devighat

APPENDIX B: DIGSILENT MODEL

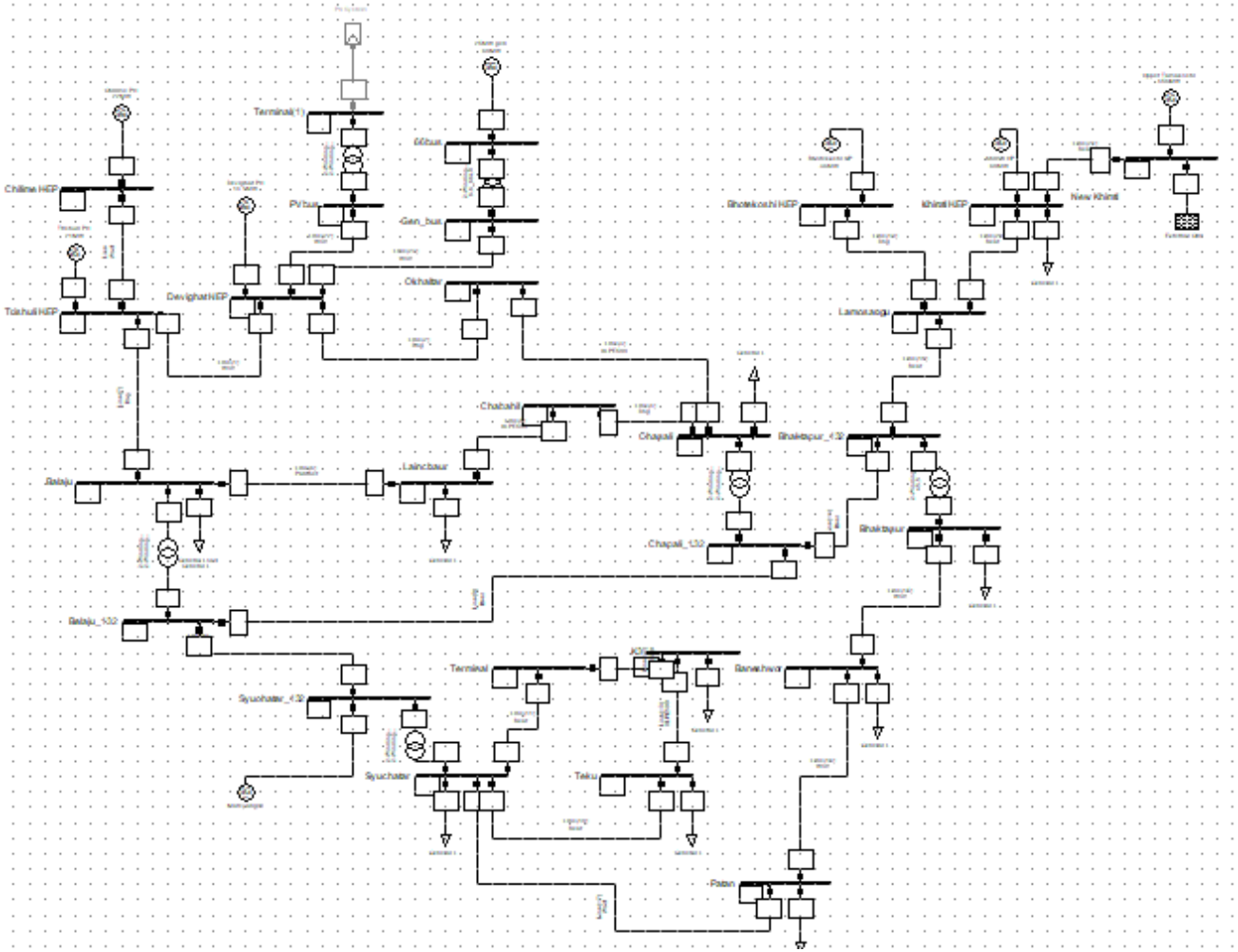

Figure B.1: DIgSILENT model for Kathmandu Valley